The 1999 Independence Day Derecho - A Modelling Study

by

Shih-Li Jou

Department of Atmospheric and Oceanic Sciences
McGill University, Montreal
August 2002

A thesis submitted to
McGill University
in partial fulfillment of the requirements for the degree of
Master of Science

Your file Votre référence
ISBN: 0-612-88227-6
Our file Notre référence
ISBN: 0-612-88227-6

Abstract

A numerical modelling of the 4-5 July 1999 derecho was performed. The storm caused over 40 million dollars of damages, several deaths and injuries across the United States and Canada. The unseasonal synoptic settings resulted in the formation of low-level moisture pooling and the buildup of convective available potential energy. The upper-level jet streak eventually furnished the trigger for the outbreak of precursor deep convection leading to the development of this derecho.

The results illustrated the feasibility of simulating the derecho using a mesoscale model with the NCEP (National Centers for Environmental Prediction) reanalysis. Convection was not initiated properly using as initial conditions the CMC (Canadian Meteorological Centre) analysis which displays less low-level moisture and potential instability, as well as downward motion over the area of convective outbreak. Similarities between the modelled profile and the environment conducive to wet microburst are discussed. Sensitivity experiments were performed to explore the effects of shallow convection, deep convective parameterization, and a different surface scheme on the simulation of the derecho.

Résumé

La modélisation numérique du derecho des 4-5 juillet 1999 a été réalisée. La tempête a causé plus de 40 millions de dollars de dommages, de nombreux décès et blessés à travers les États-Unis et Canada. L'environnement synoptique anormal pour la saison a donné lieu à l'accumulation d'humidité dans les bas niveaux et à la formation d'energie convective potentielle. Le jet en altitude a éventuellement fourni l'élément déclencheur à la manifestation de convection profonde précurseur à la formation de ce derecho.

Les résultats ont démontré la possibilité de simuler un derecho, en employant un modèle à méso-échelle avec une analyse produite par le NCEP (National Centers for Environmental Prediction). La convection n'a pas été déclenchée correctement en utilisant comme conditions initiales l'analyse du CMC (Centre Météorologique Canadien). Cette dernière contient moins d'humidité aux bas niveaux et d'instabilité potentielle, avec du movement descendant au-dessus de la région du déclenchement de la convection. Les ressemblances entre le profil simulé et l'environnement menant à la formation de micro-rafales humides sont discutées. Les expériences de sensibilité ont été réalisées pour explorer les effets de la convection peu profonde, la paramétrisation de la convection profonde, et un schéma de surface différent sur la simulation du derecho.

Table of Contents

List of Figures

List of Tables

Acknowledgements

The completion of this thesis would not have be possible without the support and the guidance of my supervisor, Dr. Peter Yau. He was always available whenever I required assistance in my research. I would like to thank him for allowing me to explore freely this fascinating storm, whose dazzling passage over Montreal has instilled an unforgettable experience in me.

The constructive inputs from members of our mesoscale research group and others were greatly appreciated. In particular, I would like to thank Badrinath Nagarajan for the many hours he spent in helping me to deal with different technical aspects of MC2. Thanks also go to Jason Milbrandt, Ron McTaggart-Cowan, Irena Paunova, Rémi Montroty, and Yongsheng Chen for contributing to my understanding of numerical modelling, programming, and other aspects.

Serge Mainville and his colleagues at the Meteorological and Environmental Service Office at Montreal provided valuable storm data, expertise, and insight on the derecho. Scientists at RPN furnished the data for the ISBA scheme, and Aldo Bellon at McGill's radar observatory provided the radar data.

I thank my friends for their moral support, which has undeniably helped

me to weather the challenging moments. I am very grateful to my parents for their unconditional encouragement. Thank you mom and dad for your support throughout these years.

Chapter 1

Introduction

1.1 Background

On the early morning of 4 July 1999 over North Dakota, severe thunderstorms originated from the foothill of the Rocky Mountains evolved into a devastating derecho, a mesoscale convective system (MCS) with violent wind gusts. For 45 minutes, sustained winds over 50 kt (93 km h^{-1}), with gusts up to 79 kt (146 km h^{-1}) (SPC, cited 2002), were reported at Fargo, North Dakota. The characteristics of the damage sustained suggest that the wind gusts could have easily exceeded 87 kt (161 km h^{-1}) over parts of Northern Minnesota. Moreover, the same region experienced widespread flooding associated with the passage of the derecho. A record breaking 110.5 mm of rain fell in just three hours at Hibbing, Minnesota. It was estimated that close to 12.5 million trees were lost over the severely hit Boundary Waters Canoe Area Wilderness in Northern Minnesota. The total property damage exceeded $30 million U.S. and several deaths and injuries were recorded (Parke and Larson, cited 2002; NCDC, cited 2002a). The damages and casualties could have been

more dramatic had the storm passed over the urban areas further south.

The derecho was travelling at 55 kt (102 km h^{-1}) over Minnesota with peak speed near 80 kt (148 km h^{-1}). It weakened into an ordinary MCS when it moved into Western Ontario. A funnel cloud was reported west of Thunder Bay (Parke and Larson, cited 2002). Several hours later, the tenacious storm re-intensified into a derecho again on entering Quebec. The windstorm raced from Western to Southern Quebec during the overnight of 4 to 5 July, generating spectacular lightning strikes. At times, the system was cruising at speeds exceeding 55 kt (102 km h^{-1}). Damages to several trees and buildings were reported, and the storm resulted in $15 million Canadian in utility repairs for Hydro-Quebec (EC, cited 2000). In addition, several deaths and injuries were reported in the U.S. and Canada (WESO, 2002; NCDC, cited 2002a).

This severe weather phenomenon took many people by surprise, especially over Quebec. In fact, storm climatology suggests that derechos are uncommon over Eastern Canada (Fig. 1.1). Also, the Canadian operational forecast models failed to predict the storm and did not recognize the convective system even after the derecho has formed. For Quebec alone, 27 severe weather bulletins associated with the passage of the storm were issued, 18 of these lied within a short period of four hours (WESO, 2002).

1.2 Definition of Derecho

Back in the late 1880's, Dr. Gustavus Hinrichs, Director of the Iowa Weather Service, proposed a specific terminology for the "Straight Blow of the Prairies" (Hinrichs, 1888). Hirinchs described this type of mesoscale system

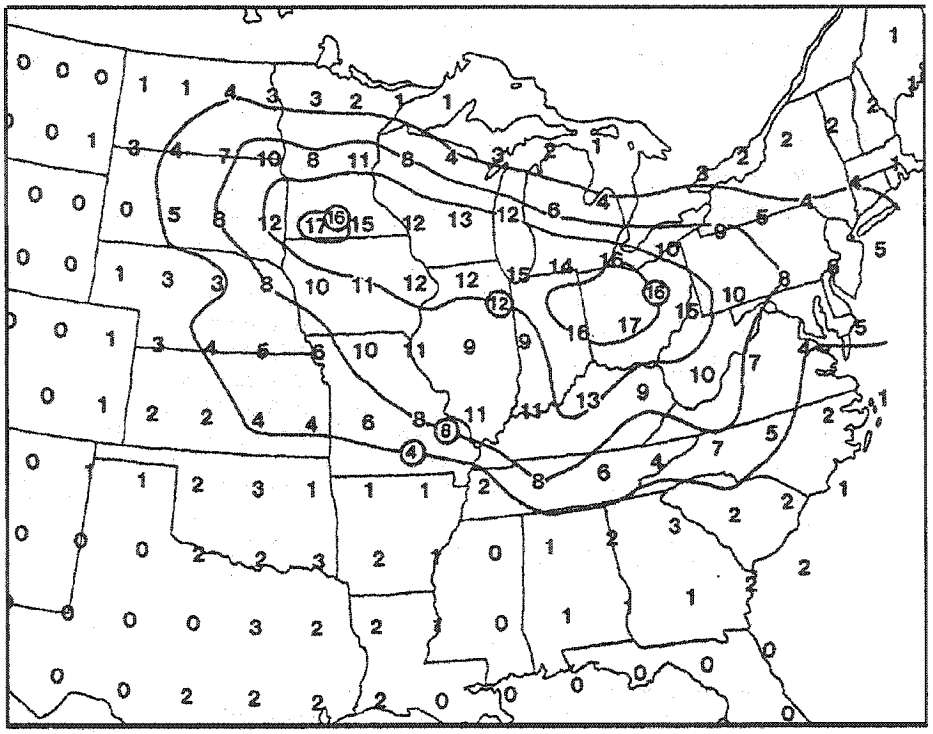

Figure 1.1: Total number of derechos in 2^o latitudes by 2^o longitudes square for the months of May through August from 1980 to 1983 (Johns and Hirt, 1987).

as "powerfully depressing and violently progressing mass of cold air, moving destructively onward in slightly diverging straight lines...". The Spanish word "derecho", meaning "straight ahead", was chosen for these windstorms, which are characterized by the non-rotating feature of their winds.

A century later, Johns and Hirt (1987), based on classification of downburst damage patterns by Fujita and Wakimoto (1981), defined derecho to include any family of downburst clusters produced by an extratropical MCS. Precisely, to be classified as a derecho, a convective storm must satisfy all the following criteria:

(1) There must be a concentrated area with convectively induced wind damage reports with wind gusts greater than 50 kt (93 km h^{-1}). The length of the major axis of the concentrated area must be at least 400 km.

(2) The reports must show spatial and temporal continuity.

(3) There must be at least three reports of Fujita scale one damages and/or wind gusts of or greater than 65 kt (120 km h^{-1}), each separated by a distance of 64 km or more.
(4) No more than three hours can elapse between successive reports.
(5) Multiple swaths of wind damage must belong to the same MCS as indicated by radars.

Derechos can be further classified as progressive or serial. Progressive derechos are frequently formed in conjunction with relatively weak synoptic features and strong convective instability. They occur mainly during late spring and summer, and display characteristics of both linear (squall lines) and nonlinear types of MCS. Serial derechos are often associated with strong surface low pressure system where dynamic lift in the synoptic environment is important. These derechos evolve from fast propagating segments of a squall line. Serial derechos can occur at any time of the year but more frequently during late winter and spring (Johns and Hirt, 1987; Bentley and Cooper, 1997; Bentley and Mote, 1998).

In a progressive derecho, the squall line is oriented nearly perpendicular to the direction of the mean wind. In a serial derecho, the squall line is oriented more or less parallel to the direction of the mean wind (Fig. 1.2). Most derechos are progressive systems and they generally move with a speed faster than that of the mean wind (Johns and Hirt, 1987).

1.3 Objectives

Contrary to other squall line producing storms, numerical simulations of derechos using real data are rare (e.g. Coniglio and Stensrud (2001)). In

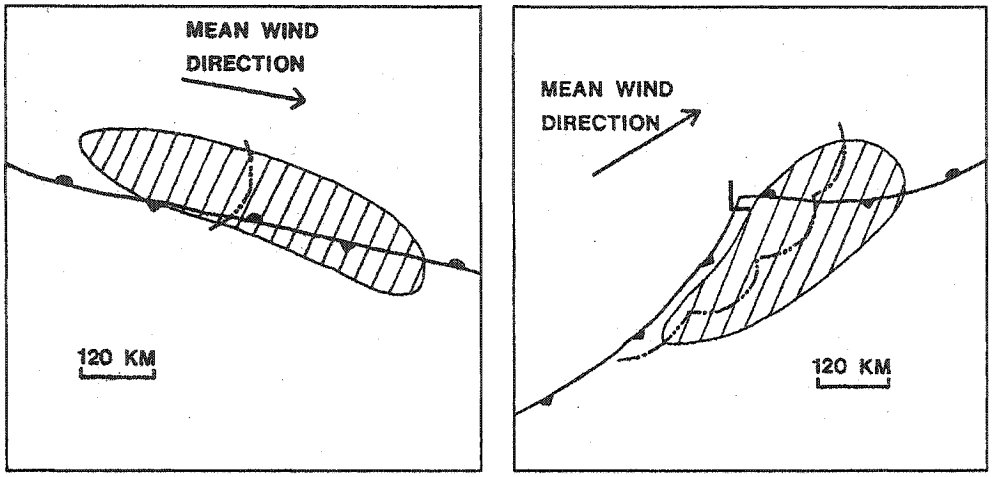

(a) (b)

Figure 1.2: Features associated with, (a) progressive, and (b) serial derecho near midpoint of lifetime. Total area affected by derecho indicated by hatching (Johns and Hirt, 1987).

this thesis, our main objectives are to examine the large-scale environment leading to the development of the 4-5 July 1999 derecho, and to demonstrate the capability of simulating the storm using a mesoscale model with real data initial conditions.

The outline of the thesis is as follows. Chapter 2 gives a detailed description of the pre-storm synoptic settings and the evolution of the storm. Chapter 3 describes the mesoscale model employed in our simulations, and the design of the experiment. The results of the simulations are presented in Chapter 4 where similarities between the modelled and the wet microburst environments are also discussed. Chapter 5 records the results of sensitivity tests. Finally, Chapter 6 presents the summary and conclusions.

Chapter 2

4-5 July 1999 Case Study

2.1 Synoptic Situation on 3 July 1999

Although the derecho affected Quebec only on 5 July 1999, the pre-storm convective activities were first observed during the local afternoon on 3 July over the Rocky Mountains. The subjective surface analysis produced by the Canadian Meteorological Centre (CMC) at 1800 UTC 3 July (Fig. 2.1) show an extensive surface ridge which dominates the southeast coast of the United States. A low pressure system is located over the North Dakota and South Dakota border with the associated warm and cold fronts stretching respectively eastward and southwestward. Significant low-level moisture behind the warm front was evident with surface dewpoints of 24°C over Illinois, Iowa, and Minnesota.

The 850 hPa NCEP (National Centers for Environmental Predictions) reanalysis of specific humidity confirmed the existence of a boundary layer moisture pool over the Great Plains states (Oklahoma, Kansas, Nebraska,

South Dakota, and North Dakota). The winds direction at this level also suggested that the humidity was transported northward from the Gulf of Mexico (Fig. 2.2). In addition, due to above normal rainfall and near normal temperatures in the previous three months (April, May, and June) over the Plains states, evapor-transpiration from the rapid growing and expanding vegetation had enhanced the moistening of the boundary layer (NCDC, cited 2002b; Parke and Larson, cited 2002). The low-level moisture advection played an important role in the initiation and the support of convective activities.

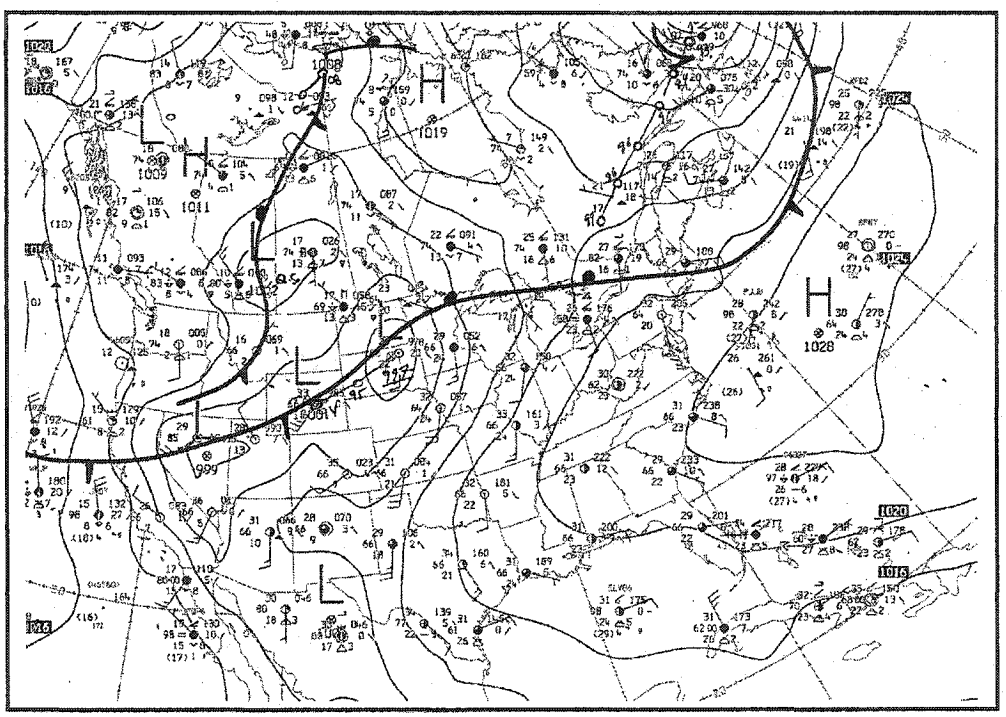

Figure 2.1: CMC subjective surface analysis at 1800 UTC 3 July 1999. Isobars are at intervals of 4 hPa (solid contours). Observations for selected stations are plotted using the standard surface observation symbols, with the temperature and the dewpoint in degree Celsius. Cold fronts, warm fronts, troughs (circle-line-circle), and centers of high (H) and low (L) pressure systems are indicated on the foreground.

At the upper level, the 500 hPa geopotential heights revealed a closed low over Southern Alberta and a broad anticyclone over Eastern United States. (Fig. 2.3). This pattern favors the formation of downslope southwesterly flow

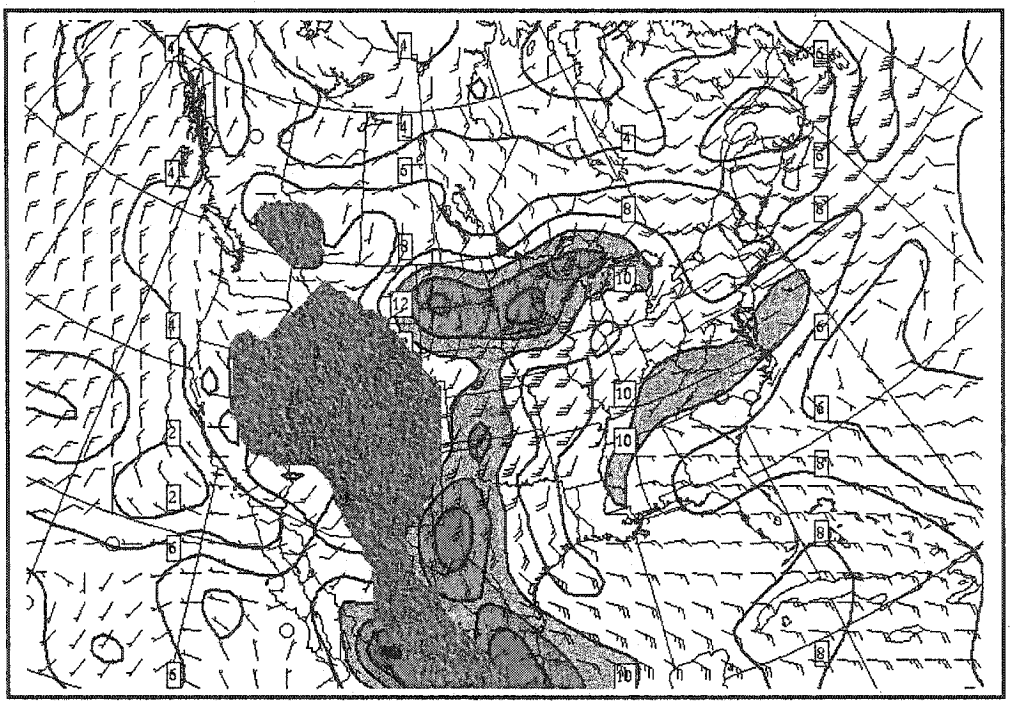

Figure 2.2: NCEP reanalysis of 850 hPa specific humidity at interval of 2 g kg^{-1} (thick solid contours) and wind vector (half barb and full bard denoting 5 and 10 kt respectively) at 1800 UTC 3 July, 1999. Areas of specific humidity greater than or equal to 10 g kg^{-1} are shaded. Relief shading indicates area below ground.

over the Rocky Mountains, resulting in adiabatic warming and drying of mid-tropospheric air east of the mountains. Moreover, satellite observation and surface station reports indicated that the sky was clear over the Rockies on 3 July. Hence, daytime solar heating over the mountains also contributed to warming the mid-tropospheric air (Bluestein, 1993). The combined heating effects resulted in an unusually warm air layer at 700 hPa over part of the Eastern Rockies and the Plains states (Fig. 2.4).

The warm air steepened the lapse rate and reduced the static stability in the lower mid-troposphere, which in turn increased the amount of convective available potential energy (CAPE). In addition, this large-scale 700 hPa warm air acts as a lid on top of the low-level moist air, thereby inhibits the convective transport out of the boundary layer, and enhances the pooling of moisture therein (Bluestein, 1993). The presence of dry mid-level air is an important

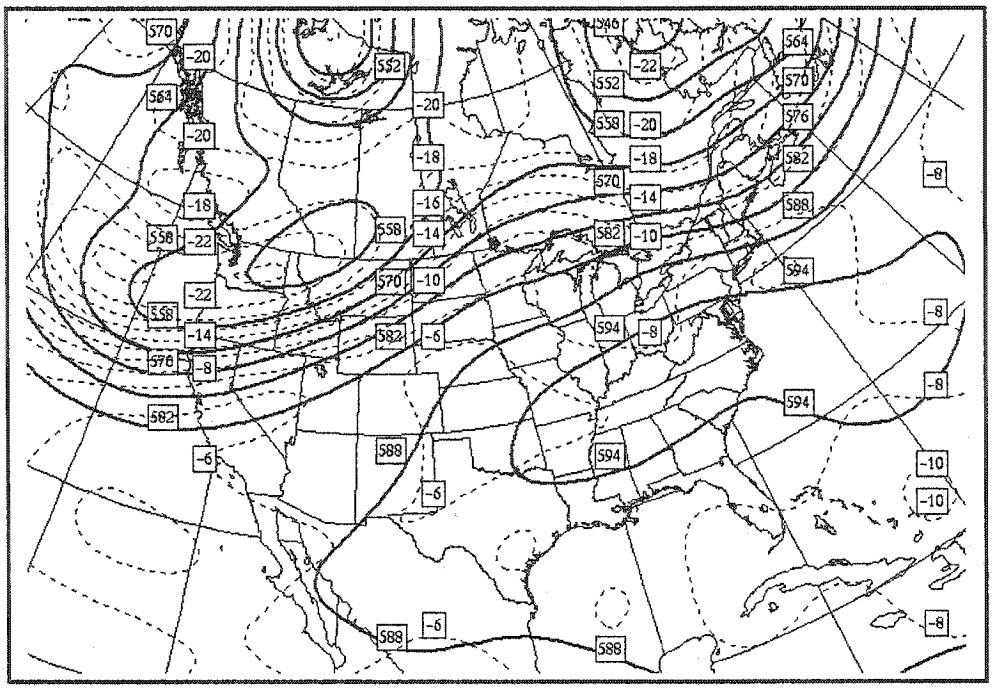

Figure 2.3: NCEP reanalysis of 500 hPa geopotential height (thick solid contours) at intervals of 6 dam and temperature (thin dashed contours) at intervals of 2°C at 1800 UTC 3 July 1999.

factor in the development of strong wind gusts from convective downdrafts, as the cooling arising from the evaporation of precipitation falling into the unsaturated air enhances the negative buoyancy (Johns and Doswell III, 1992; McNulty, 1995). Furthermore, Figure 2.4 also indicates warm advection over the Plains states, consistent with the finding of Johns and Hirt (1987) who identified in 96% of their cases, the presence of 700 hPa warm air advection within a radius of 320 km of the location of initiation of the derecho.

At 1800 UTC over the Plains, large-scale lifting of air parcel for deep cumulus convection was inhibited because it lied under the right-exit region of an upper-level jet streak (Fig. 2.5) and is subject to large-scale subsiding motion.

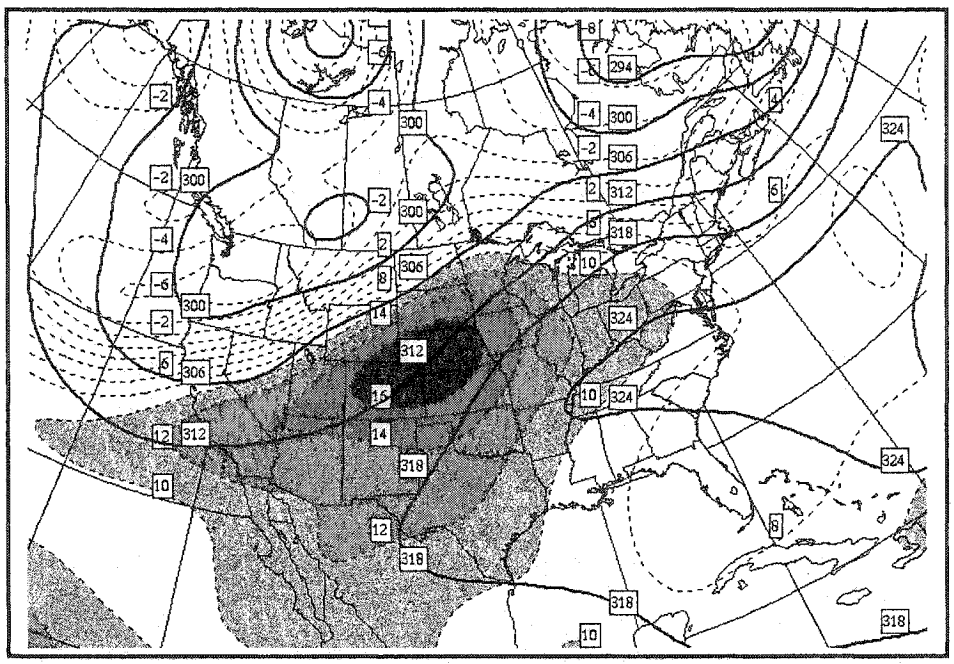

(a)

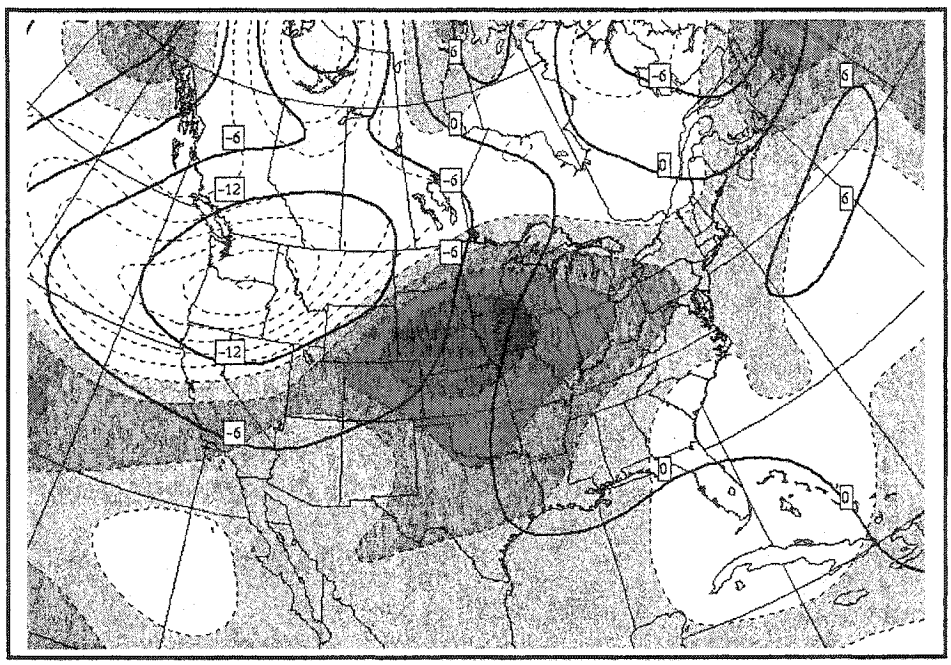

(b)

Figure 2.4: NCEP reanalysis of 700 hPa geopotential height (thick solid contours) at intervals of 6 dam and temperature (thin dashed contours) at intervals of 2°C, (a) at 1800 UTC 3 July 1999, with shaded areas denoting temperature greater than or equal to 10°C, (b) departures of the daily average values for 3 July 1999 from the 40 years (1957-1996) climatological values for the month of July, with shaded areas denoting positive temperature anomalies.

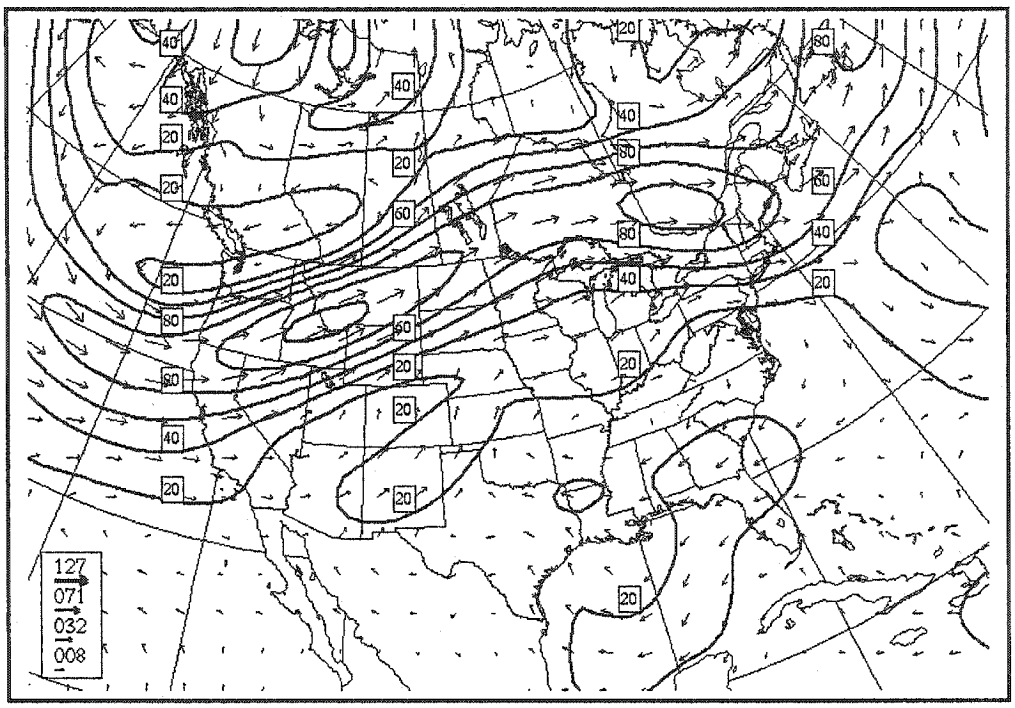

Figure 2.5: NCEP reanalysis of 300 hPa winds vector and wind speed (thick solid contours) at intervals of 20 kt at 1800 UTC 3 July 1999.

2.2 History of the Storm

The description of the event is constructed with data collected from various sources, including the U.S. Next Generation Weather Radar (NEXRAD) national mosaic reflectivity maps, satellite imagery, meteorological report aviation routine (METAR) observations, upper-air soundings, U.S. Storm Prediction Center (SPC) and Environment Canada (EC) severe weather bulletins, and the article by Parke and Larson (cited 2002).

The life time of the storm can be classified into different stages. The convective initiation stage covers the period around 1800 UTC 3 July to 1200 UTC 4 July. The first derecho stage spans from 1200 UTC to 1800 UTC 4 July. The derecho then weakens from 1800 UTC 4 July to 0100 UTC 5 July. It then re-intensified into a second derecho stage from 0100 UTC to 1000 UTC

5 July.

2.2.1 Convective Initiation

On 3 July 1999, isolated elevated deep convective activities were initiated over the Colorado Rockies during the local mid-afternoon (1800 UTC). Convection propagated slowly downslope and by the late afternoon (2300 UTC), it had expanded into Southeastern Wyoming and the Nebraska Panhandle . The environment favorable for elevated convection is characterized by an inverted "V" sounding on a skew T-log p diagram (Bluestein, 1993; Johns and Doswell III, 1992), as depicted in the Grand Junction (GJT) sounding in Figure 2.6(a). The boundary layer was deep, and the well-mixed layer extended from the surface up to about 550 hPa. The temperature profile followed closely the dry adiabats. The dewpoint curve was parallel to lines of constant mixing ratio.

The three upper-air soundings closest to the downstream path of the convective cells at 0000 UTC 4 July displayed similar features: a well-mixed boundary layer with near dry adiabatic lapse rate, a very stable layer (cap) near 800 hPa, and a value of CAPE ranging between 231 and 966 J kg^{-1} (Figs. 2.6(b) - (d)). The CAPE were calculated for a parcel corresponding to a $\sim$50 hPa layer averaged temperature and dewpoints, excluding the surface layer. In all these soundings, the temperature profiles with near dry adiabatic lapse rate and the winds of 10 kt or more suggest a well mixed boundary layer. Therefore, the moist layer at the surface in Figures 2.6(b) - (d) should not occur. It has been documented that the age and the packaging of the radiosounds can cause these erroneous readings (Guichard et al., 2000). Nevertheless, the characteristics of these mid-tropospheric soundings

are consistent with the synoptic setting described in section 2.1.

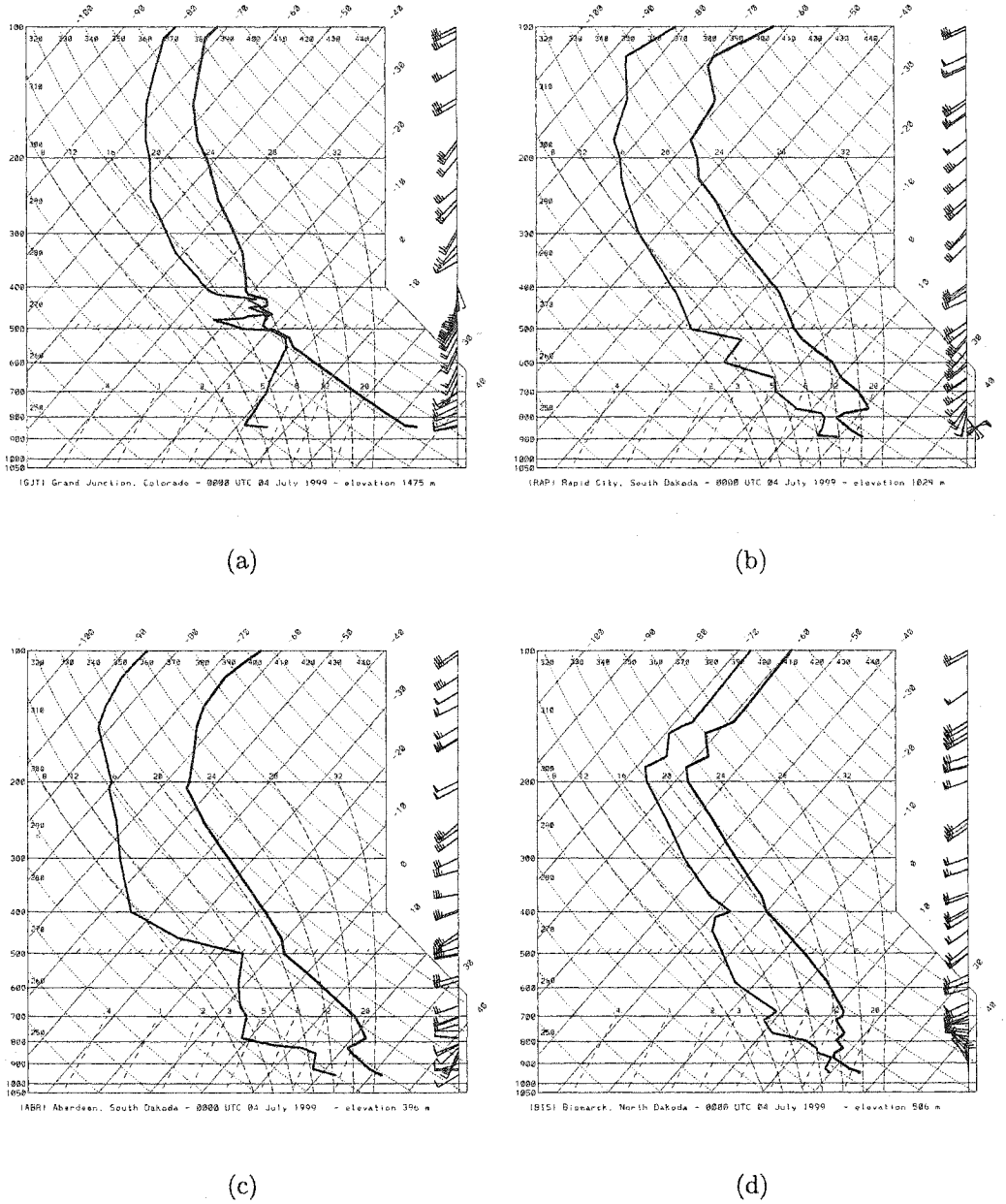

Figure 2.6: Observed upper-air sounding at 0000 UTC 4 July 1999 at, (a) Grand Junction (GJT), with CAPE of 188 J kg^{-1}, (b) Rapid City (RAP), with CAPE of 409 J kg^{-1}, (c) Aberdeen (ABR), with CAPE of 966 J kg^{-1}, (d) Bismarck (BIS), with CAPE of 231 J kg^{-1}. Wind vectors are shown with the half barb, full bard, and flag denoting 5, 10, and 50 kt respectively. Location of the sounding stations are shown in Figure 2.7.

The development of the nighttime low-level (850 hPa) southerly jet over

the Plains (Fig. 2.2) enhanced the moisture convergence ahead of a frontal zone near the South Dakota-Nebraska border. Previous studies on derechos have identified moisture advection as a prominent feature south of the region of genesis of mesoscale convective systems (MCSs) during their formative stage (Bentley and Cooper, 1997). It is also the main source of instability for elevated storms (Bernardet and Cotton, 1998).

As the thunderstorms continued to move northeastward into South Dakota, the term "bowing" and "MCS" were first used by SPC to describe the storm at 0618 UTC 4 July. By then the convective activities have evolved into an organized mesoscale system with a bowing radar echo structure. Meanwhile, a line of thunderstorms developed further northwest near the South Dakota-North Dakota border, ahead of a cold front. Three hours later, the line of thunderstorms and the MCS merged, and at about 1200 UTC the storm became a derecho. Hereon, the storm will be designated as the Independence Day derecho (ID2).

2.2.2 First Derecho Stage

According to Parke and Larson (cited 2002), the MCS intensified rapidly at around 1200 UTC 4 July. The 500 hPa short wave originated from the Montana-Wyoming region had deepened as it reached North Dakota. The temperature field at 500 hPa was characterized by a warm intrusion over Western North Dakota and a cold intrusion over Northern Minnesota. This pattern produced a strong mesoscale baroclinic zone over Northern Minnesota (Fig. 2.7).

Analysis of the METAR reports indicates a surface moisture pool with dewpoints ranging from 23 to 25^{o}C located over Central and Southern Min-

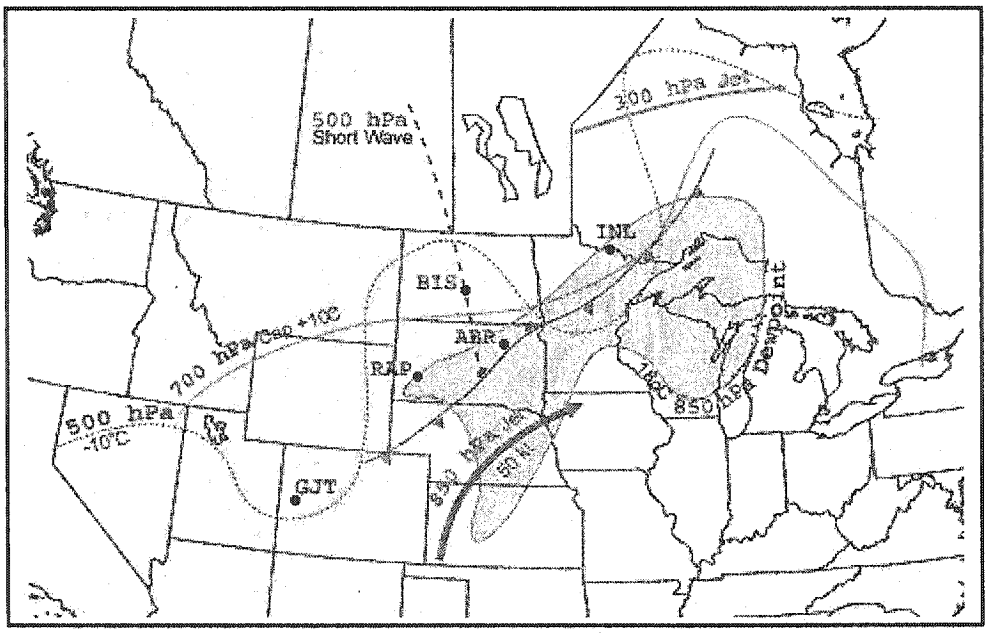

Figure 2.7: A composite of the 1200 UTC 4 July 1999 synoptic setting featuring positioning of the 300 hPa jet, 500 hPa short wave through and -10°C isotherm, 700 hPa 10°C isotherm, 850 hPa jet and dewpoint of 18°C or greater in shaded zone, and surface fronts (Parke and Larson, cited 2002). Black dots denote upper-air sounding stations (GJT, RAP, ABR, BIS, and INL).

nesota, east-southeast of ID2. As the winds were blowing from the high humidity region into ID2, the moisture advection supports the development of the storm. The atmosphere was strongly destabilized with the cold air intrusion in the mid-upper atmosphere on top of the initially well-capped warm moist air in the lower levels (Parke and Larson, cited 2002). Due to the small scale of the phenomenon, it was not possible to observe these features from the NCEP reanalysis data, which has a horizontal resolution of 2.5° (refer to Chapter 3 for more details on the NCEP reanalysis).

Satellite imagery at 1200 UTC depicted ID2 over Eastern North Dakota, with the anvil extending into Southeastern Manitoba and extreme Western Ontario (Fig. 2.8). The radar reflectivity composite (not shown) indicated precipitation covering most of Eastern North Dakota. A quasi-stationary southwest-northeast oriented thermal boundary was located south of the storm

(Fig. 2.7), a feature identified by Johns and Hirt (1987) as essential in the formation of derechos due to the proximity of low-level warm advection near the thermal boundary.

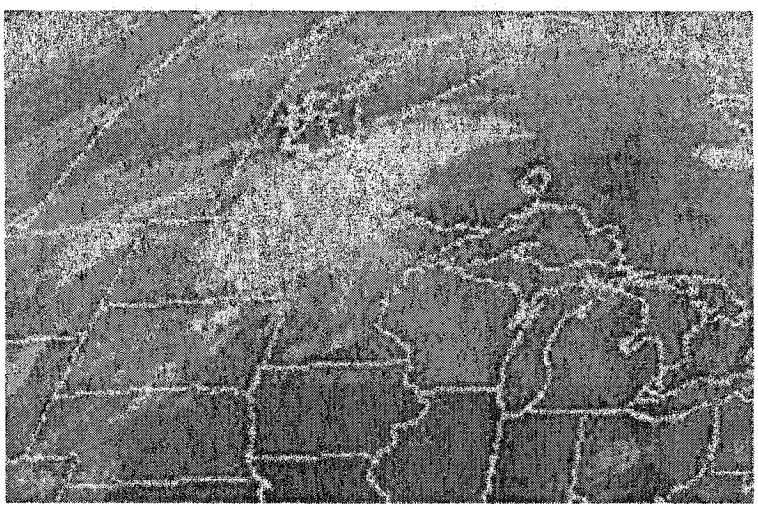

Figure 2.8: Infrared satellite image at 1200 UTC 4 July 1999 showing ID2 over North Dakota.

Wind gusts up to 79 kt (146 km h^{-1}) were reported as ID2 moved from North Dakota into Minnesota. On approaching Western Ontario, the storm was travelling at near 80 kt (148 km h^{-1}), a speed higher than the environmental winds between the surface and 300 hPa (Parke and Larson, cited 2002). ID2 lost its derecho characteristics shortly after it entered Ontario when the wind gusts diminished to less than 50 kt. At around 2200 UTC 4 July, ID2 landed over the eastern shore of Lake Superior, after crossing over the large body of relatively cold water. According to the Great Lakes Surface Environmental Analysis (GLSEA) data, the daily average surface water temperature for Lake Superior was around 7°C (GLSEA, cited 2002). Surface stations north of the lake, on the other hand, reported southwesterly winds and dewpoints in the 18-20°C range prior to the arrival of ID2. This suggested that the low-level moist air had overrun the cold shallow boundary layer located just above the surface of the lake. However, these dewpoint values are lower

than those over Minnesota and the findings from Johns and Hirt (1987).

The cold lake temperature and the lower dewpoint temperatures may explain the transition of ID2 to a non-derecho MCS. Nevertheless, the storm was still in the area with elevated dewpoints at 850 hPa shown in Figure 2.7. The continuous presence of moist air on the east-southeast side of the storm is a common observed feature in derechos (Johns and Hirt, 1987; Bentley and Cooper, 1997).

2.2.3 Second Derecho Stage

ID2 re-intensified and regained the derecho status as it entered Western Quebec between 0100 and 0200 UTC 5 July. Its speed accelerated to 50 kt (93 km h^{-1}) (Mainville et al., 2001). Surface dewpoints were between 22 and 25°C over Southern Quebec before the arrival of the windstorm. Precipitation associated with the derecho was first observed by the McGill radar just before 0500 UTC and the system was out of radar coverage shortly after 0830 UTC. Doppler radial velocities were over 54 kt (100 km h^{-1}) as the storm moved across Montreal. The bowing segment of ID2 was characterized by radar reflectivity in the range of 45 to 55 dBz at an altitude of 2.5 km. An area of trailing stratiform precipitation was also detected from the radar. As the storm passed over Montreal, the McGill wind profiler registered significant downward motions on the order of several hundreds of cm s^{-1} from the surface up to about 8 km above ground (Fig. 2.9). The maximum downward velocities were of the order of 800 cm s^{-1}. The profiler data also suggested that the storm was dominated by downdrafts during this stage. Over Quebec, the highest recorded wind gusts of 62 kt (115 km h^{-1}) were reported at Sherbrooke airport (YSC) at 0745 UTC 5 July. According to EC, wind gusts up to (160

km h^{-1}) might have occurred over some areas.

SPC estimated the travelling speed of ID2 at 60-65 kt (111-120 km h^{-1}) as it entered the mountainous region of New Hampshire and Maine. The last severe thunderstorm watch issued for ID2 was cancelled by 1045 UTC 5 July, as the storm weakened over Maine. The interaction of ID2 with the elevated topography of the Appalachian Mountains and the lack of low-level moisture probably contributed to its dissipation.

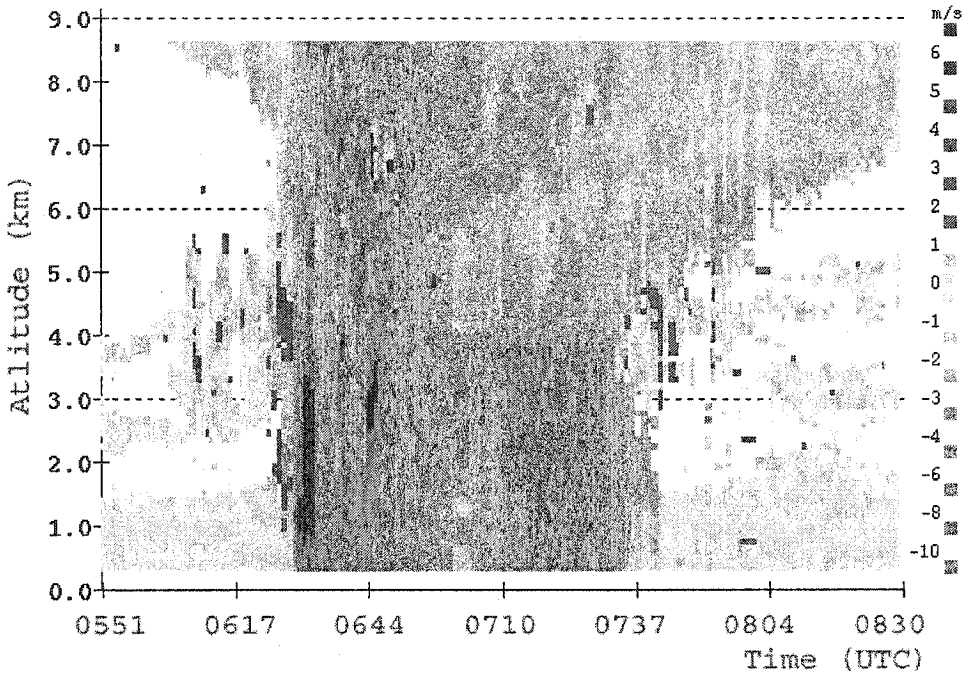

Figure 2.9: Observed vertical motion (m s^{-1}) from the McGill profiler between 0551 UTC and 0830 UTC 5 July 1999.

Chapter 3

Model Specification

For this study, the simulations were performed using the Mesoscale Compressible Community (MC2) model. Developed at Recherche en Prévision Numérique (RPN), a division of Meteorological Research Branch of Environment Canada, the model is characterized by the application of semi-implicit semi-Lagrangian method. The description of the model specifications follows the documentation by Benoit et al. (1997).

3.1 Model Dynamics

The limited-area non-hydrostatic MC2 model resolves the fully compressible Euler equations, normally on a polar stereographic projection true at 60°N. The semi-implicit scheme solves implicitly the fast propagating waves, such as acoustic waves, whereas the slow propagating waves are handled explicitly. The discretization of spatial derivative employs finite differences on a three dimensional staggered grid, featured in the horizontal by an Arakawa

C-grid and in the vertical by a Tokioka B-grid. The use of an isothermal reference state increases the numerical stability of the semi-implicit scheme. In principle, the semi-Lagrangian scheme is stable even when the Courant number exceeds one.

In the model, orography is accounted for by the use of the terrain-following Gal-Chen height coordinate, with the introduction of variable vertical grid spacing. The adjustable height levels allow a higher vertical resolution in the lower atmosphere. The vertical coordinate surfaces gradually flatten out with height such that the model top is horizontal. The boundary condition at the model top is zero vertical motion, and a sponge zone under the model lid can be applied to absorb the upward propagating waves. Similarly, the model surface is constrained to the boundary condition of zero vertical displacement on a Gal-Chen surface.

3.2 Model Physics

The MC2 is interfaced with the complete RPN physics package, which is shared by all the Canadian Meteorological Centre (CMC) operational models and RPN research models. The package is updated continuously and it allows the choice of several parameterization schemes and physical processes.

For most of our model runs, a heat budget based force-restored scheme is used to predict the land surface temperature and the soil moisture. The soil moisture availability factor is supplied by the initial conditions for the computation of surface soil evaporation. The scheme imposes a closure condition for heat and water balance at the air-soil interface, and assumes diffusive processes for the unknown subsurface ground fluxes (Benoit et al., 1989).

Throughout the integration, the temperature of the water surface is held constant.

For sensitivity studies, the Interactions Soil-Biosphere-Atmosphere (ISBA) surface scheme was also used. This scheme is based on the original work of Noilhan and Planton (1989). Two categories of entry parameters are required by the scheme. The primary parameters include the percentage of sand and clay soil, vegetation type, and the land-water mask. The secondary parameters describe the physical characteristics of the soil and vegetation. The goal of this scheme is to determine the lower boundary conditions for vertical diffusion of temperature, moisture, and momentum. Prognostic variables of soil temperature and moisture, moisture retained on foliage of vegetation, ground snow characteristics, as well as the hydrological budget of the surface are evaluated.

The mixing within the planetary boundary layer is treated with a prognostic equation for turbulent kinetic energy. Vertical diffusion is used for the parameterization of turbulence induced vertical transfers.

The radiation parameterizations are fully interactive with clouds. The effects of water vapor, carbon dioxide, ozone, and clouds are included both in the infrared radiation scheme and in the solar radiation scheme. The latter also considers the physical processes of Rayleigh scattering and multiple scattering.

The grid-scale resolvable precipitation is treated with the modified explicit microphysics scheme developed by Kong and Yau (1997). In addition to warm rain and ice-phases processes within the original package, the version used for this study includes also hail/graupel processes. The scheme solves explicitly the equations for cloud water, rain water, and ice or snow mixing

ratio, together with the calculation of the source and sink term, as well as the advection and sedimentation of hydrometeors. The source and sink terms are formulated based on the bulk-water method, and include condensation and evaporation, auto-conversion, accretion, heterogeneous and homogeneous nucleation of ice nuclei, deposition and sublimation, as well as freezing and melting.

For the treatment of parameterized clouds, a number of convective schemes are used for this study: the Betts-Miller shallow and deep convection scheme (Betts and Miller, 1993), the Kuo scheme (Mailhot et al., 1998), and the Kain-Fritsch scheme (Kain and Fritsch, 1993).

The parameterization of boundary layer clouds is performed by using the Betts-Miller shallow convection scheme. This parameterization is based on convective adjustment toward a reference quasi-equilibrium structure. The method computes a first-guess moisture reference profile with linearized slope of mixing line within the cloud. Corrections are applied to the first-guess values to satisfy the constraints of zero condensation rate and zero precipitation rate when integrated vertically. Hence, the scheme is non-precipitating but transports vertically heat and moisture.

The Betts-Miller deep convection scheme follows the same principle as the shallow convective scheme of quasi-equilibrium. The first-guess moisture profile is computed from the first-guess thermal reference profile, then both profiles are corrected to satisfy the constraint of moist static energy balance. If no precipitation is produced by the convective adjustment, the shallow convective scheme is employed instead.

For the Kuo deep convection scheme, the presence of conditionally unstable layer combined with moisture convergence, resulting from large-scale

forcing and surface evaporation, triggers cumulus cloud formation. Part of the net moisture convergence humidifies the environment, while the remaining moisture warms the environment by condensation and falls in the form of precipitation.

The Kain-Fritsch convective parameterization uses an entraining-detraining cloud model. The scheme is based on the removal of convective available potential energy within an advective time window in a grid area. The advective period is a predefined estimate of the time required for clouds to move through a grid box, and the characteristics of the clouds are assumed unchanged during this period (Fritsch and Kain, 1993). The trigger function requires that a buoyant updraft parcel must be able to reach the lifting condensation level (LCL), and the resulting cloud must be sufficiently deep before convection is set off.

3.3 Nesting and Initialization

Because MC2 is a limited-area model, supplies of lateral and upper boundary conditions are required at every time step. Nesting in the horizontal and vertical of all predictive variables is performed over a sponge zone after every dynamics time step, with the exception of hydrometeor water contents. An attenuation function incorporates smoothly the nested (boundary) values with the non-nested (model) values, providing the sponge zone contains enough grid points from the boundary. The nested values have their maximum weight at the boundary, and minimum weight at the interface between the sponge zone and the internal free domain. Different attenuation functions are defined for the lateral and the vertical sponge zones. Vertical nesting is not applied if the nesting layer is below the topmost momentum level.

Since nesting values are required for all time interval during the entire integration, linear interpolation of consecutive nesting data sets is performed to provide the nesting values at every time step. Output data from large-scale models, dataset from objective analyses, or output data from a previous MC2 model run can be the source of nesting data. For the MC2 model, the capability of self-nesting enables high resolution simulations starting with coarse resolution analysis, which can often be the only initial data available.

MC2 uses dynamic initialization by applying a small forward integration in time, follow by a backward integration to the starting time. The process is particularly useful when the initial vertical motion is not supplied, the balance state is not present in the input data set, or the balance state is not compatible with the numerical balance of MC2. Initialization also reduces the spurious pressure oscillations in early integration, and the spin-up problem related to condensation.

Simulation mode or self-sufficient forecast mode can be chosen for running MC2. Sets of objective analyses or model output are required to provide boundary conditions for the simulation mode. For forecast mode, only the analysis field is provided initially, and no lateral or upper boundary condition is supplied to the model afterward during the integration. As long as the domain of simulation is away from the equator, MC2 can operate in the true forecast mode for about two days.

CMC global analysis and NCEP reanalysis fields are used as initial and boundary conditions for this study. These datasets are products of different global data assimilation systems.

The Canadian global data assimilation system was used to produce the CMC global analysis (Mitchell et al., 1993, 1996). At every 6-hour, the system

performs a 6-hour forecast from a T79 global spectral forecast model with 21 vertical levels, a multivariate 3D statistical interpolation analysis on a global Gaussian grid, and a non-linear normal-mode initialization (NNMI) to eliminate spurious large-amplitudes gravity waves in the next 6-hour forecast. The 0.9^o horizontal resolution analysis data contain the fields of geopotential height, temperature, dewpoint depression, and horizontal winds on the following 16 isobaric levels: 1000, 925, 850, 700, 500, 400, 300, 250, 200, 150, 100, 70, 50, 30, 20, and 10 hPa.

The NCEP reanalyses are generated by the NCEP/National Center for Atmospheric Research (NCAR) reanalysis system, which contains a data preprocessor module, a data assimilation module, and an archive module (Kalnay et al., 1996). The central module of data assimilation system is mainly composed of a T62 global spectral model with 28 vertical levels, a spectral statistical interpolation analysis system without NNMI, and a one-way coupled ocean model. The reanalysis data of 2.5^o horizontal resolution include the fields of geopotential height, temperature, specific humidity, and horizontal winds on the same levels as the CMC analysis, with the addition of an extra level at 600 hPa.

The simulations were run with version 4.9.1 of MC2 and version 3.66 of the RPN physics package on the NEC SX-4 supercomputer located at CMC.

Chapter 4

Results

4.1 Model Settings

The simulations were divided into two parts: a coarse run followed by a nested run. The main objective of the coarse simulation was to provide the initial and the boundary conditions to the nested run, by generating the necessary fields at an intermediate resolution between the 2.5^o horizontal resolution NCEP reanalysis and the higher resolution mesoscale nested run. The coarse simulation was done using an 80-km horizontal resolution domain with 80 by 50 grid points (Fig. 4.1). The choice of this domain was determined after a series of preliminary sensitivity experiments to determine the optimal configuration for adequately simulating the upper-level jet exiting the north-east corner of the domain. The vertical resolution was defined by 40 Gal-Chen levels, with the model top at 31 km. A 45-hour simulation was performed, from 1800 UTC 3 July to 1500 UTC 5 July 1999. The NCEP reanalysis atmospheric data were used for the initial and the boundary conditions, while the initial surface boundary conditions were provided by the CMC analysis

and climatological data. The lateral boundary conditions were supplied every six hours. The time step was 600 s, and the output was generated every three hours.

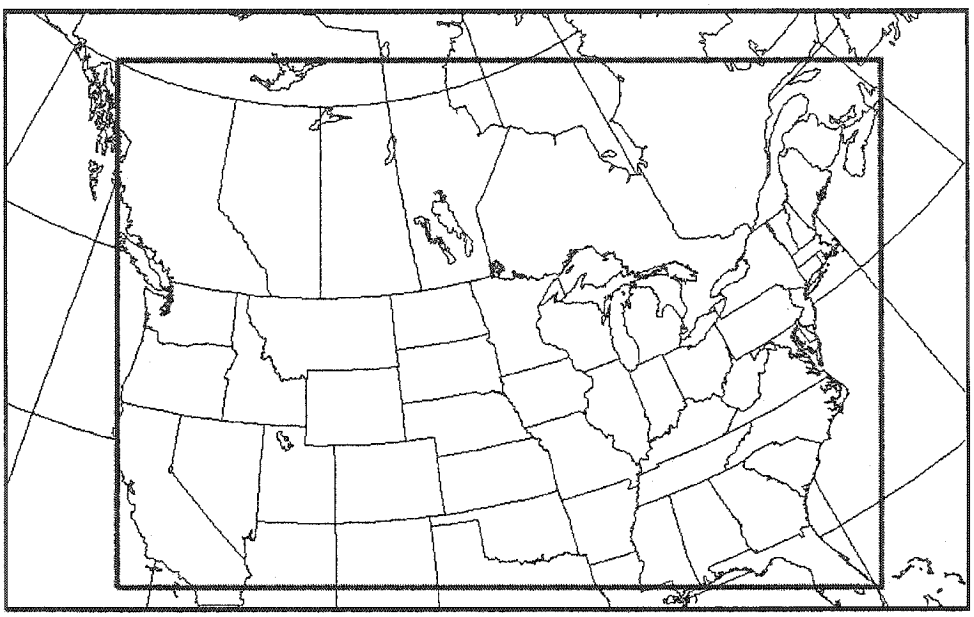

Figure 4.1: 80-km horizontal resolution domain (outer box) and 25-km horizontal resolution domain (inner box).

The Kuo and the Betts-Miller deep convection schemes, with or without the Betts-Miller shallow convection scheme, were used to determine the optimal convective parameterization to be applied for the coarse run. The combination of the moisture-convergence-based Kuo scheme with the Betts-Miller shallow convection scheme produced the most realistic results. In fact, all the combinations with the Betts-Miller deep convection scheme failed to initiate the storm. This conclusion confirmed the role of large scale moisture convergence as one of the main ingredients for the development of derecho (Johns and Hirt, 1987; Bentley and Cooper, 1997).

To adequately resolve the mesoscale feature of the derecho, a nested run at 25-km horizontal resolution was performed. The domain is defined by

200 × 130 grid points, with 40 vertical levels (Fig. 4.1). The initial and the boundary conditions were obtained from the output of the 80-km coarse simulation, with the lateral boundary conditions updated every three hours. To keep the Courant number below one, the time step was reduced to 120 s. A 36-hour simulation was made, from 2100 UTC 3 July to 0900 UTC 5 July. The Kain-Fritsch deep convection and the Betts-Miller shallow convection schemes were used.

4.2 Validation of the Results

To validate the 80-km results, qualitative comparisons were made with radar maps, satellite imagery, and the NCEP reanalysis. For the 25-km run, more quantitative comparisons were made. The following sections focus on details of the 25-km validation.

4.2.1 Convective Initiation and Stage One of Derecho

The radar composites were the primary data used to compare with the mesoscale features from the simulations. The precipitation rate obtained from the model was converted into radar reflectivity using the Z-R relationship employed by the U.S. NEXRAD system (Fulton et al., 1998),

$$Z = 300R^{1.4}, \tag{4.1}$$

where $10 \log Z$ is the reflectivity factor in dBz, and R is the rain rate in mm h^{-1}. It should be remarked that the NEXRAD composite was produced by taking the maximum reflectivity within a vertical column above each point in the radar coverage. Thus, the composite might not necessary give the actual

precipitation rate at the surface. However, it provides a good estimate of the precipitation coverage and maximum intensity over a large area.

At 0300 UTC 4 July, the modelled deep convective cells were situated over Wyoming, the Montana-Wyoming border, and the Wyoming-Nebraska-South Dakota border (Fig. 4.2(a)). The location of the modelled storms shows a westward bias relative to the observed storms (Fig. 4.3). During the hours following 0300 UTC, the simulated cells moved northeastward, and they merged before entering North Dakota. The trajectory of the newly formed storm eventually brought the storm system to a location close to the observed derecho over North Dakota at 1200 UTC. When compared with the radar composites at 0600 UTC and the 0900 UTC, we note that the model produced a much weaker line of thunderstorm north of the derecho (indicated by the arrow in Fig. 4.2(c) and in Fig. 4.3(c)). This discrepancy did not have a significant short-term impact on the survival or the evolution of the simulated derecho. At 1200 UTC, the simulated maximum reflectivity was slightly east of that depicted in the radar composite. At a horizontal resolution of 25 km, the model obviously was not able to resolve the small areas of peak maximum reflectivity ranging from 45 to 60 dBz. However, the 35 to 45 dBz contours from the simulation cover an area comparable to the radar observations.

Figure 4.4 shows the convective and stratiform precipitation rates at the surface at 1200 UTC 4 July. Convective precipitation occurs mostly at the leading edge of the storm and stratiform precipitation occurs mainly at its rear. Figure 4.5 indicates a strong leading convective updraft. Behind the leading deep convection, a secondary weaker and shallower updraft region is found. This updraft zone corresponds to the zone of maximum stratiform precipitation rate at the time (Fig. 4.4) and may represent the remnant of

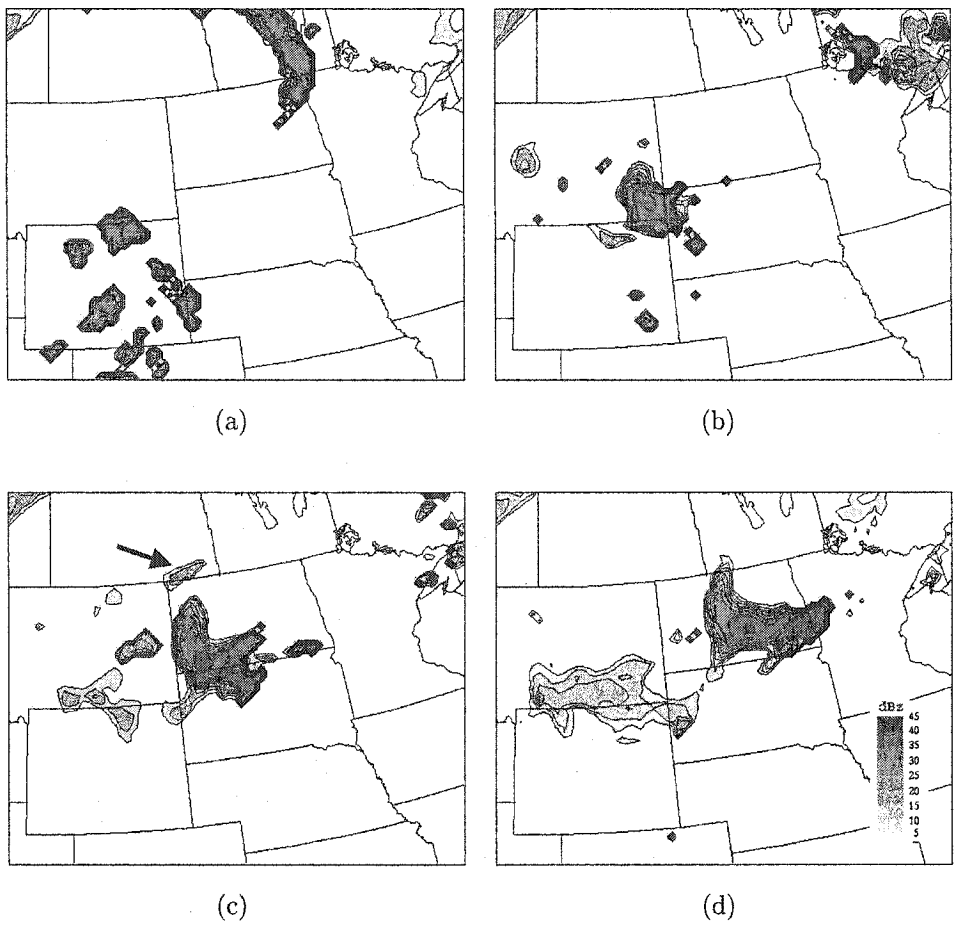

Figure 4.2: Radar reflectivity (dBz) computed from the nested run modelled precipitation rate for, (a) 0300 UTC, (b) 0600 UTC, (c) 0900 UTC, and (d) 1200 UTC 4 July.

an earlier convective cell. Slightly to the west of the secondary updraft, a downdraft region occurs at low levels. Figure 4.6 illustrates the storm relative flow, which shows little tilting in the leading deep convective updraft. Most of the cloud water is found between 5 and 7 km above the ground over the region of the secondary updraft. West of the secondary updraft, the circulation below 4 km suggests that the low-level front-to-rear flow was overrunning a low-level cold pool.

A vertical cross-section of equivalent potential temperature (Θ_e) indicates a high Θ_e (warm) pool in front of the derecho (Fig. 4.7), creating a region

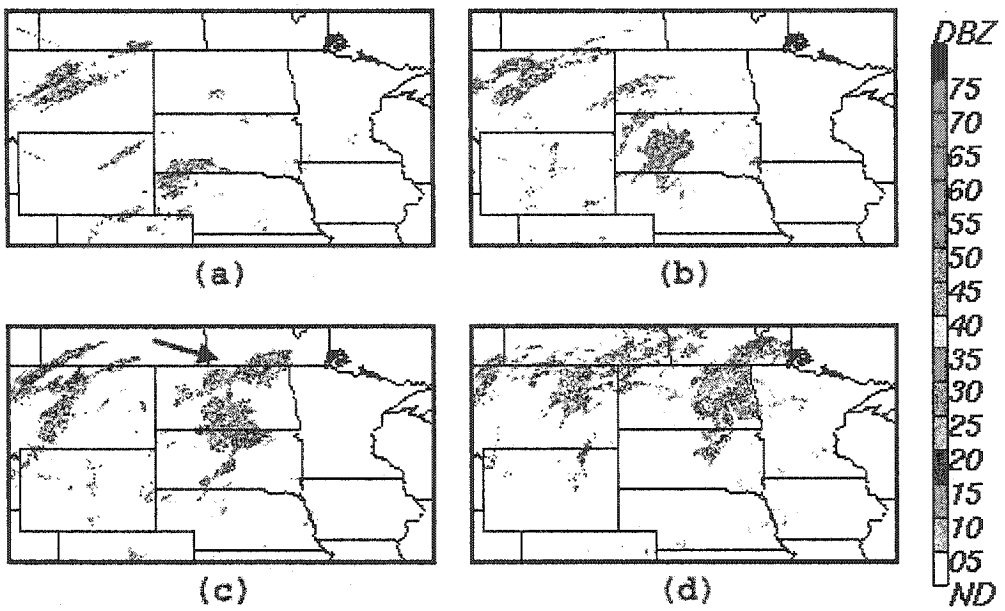

Figure 4.3: NEXRAD radar composite (dBz) for, (a) 0300 UTC, (b) 0600 UTC, (c) 0900 UTC, and (d) 1200 UTC 4 July.

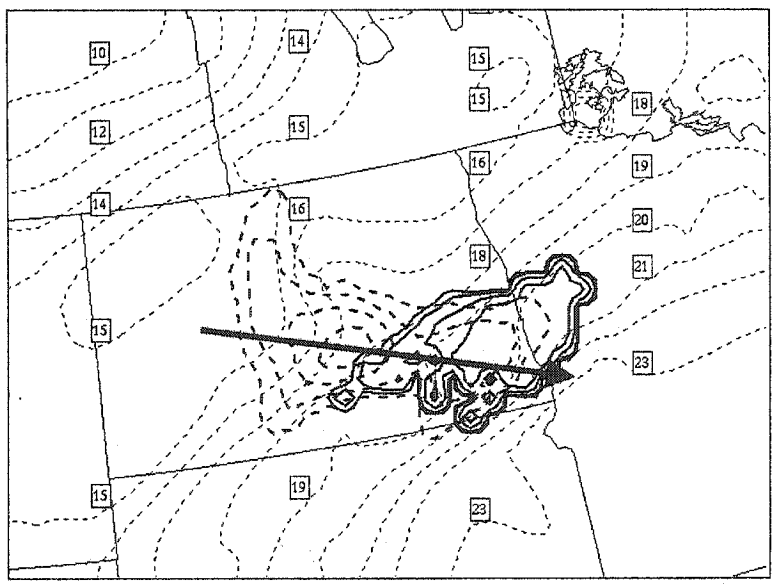

Figure 4.4: Convective precipitation rate (thick solid contours) and stratiform precipitation rate (thick dashed solid contours) at intervals of 1, 2, 5, and 10 mm h^{-1}, and surface temperature (thin dashed contours) at intervals of 1°C from the nested simulation at 1200 UTC 4 July. The thick arrow denotes the location of the vertical cross-sections shown in Figure 4.5 and Figure 4.6.

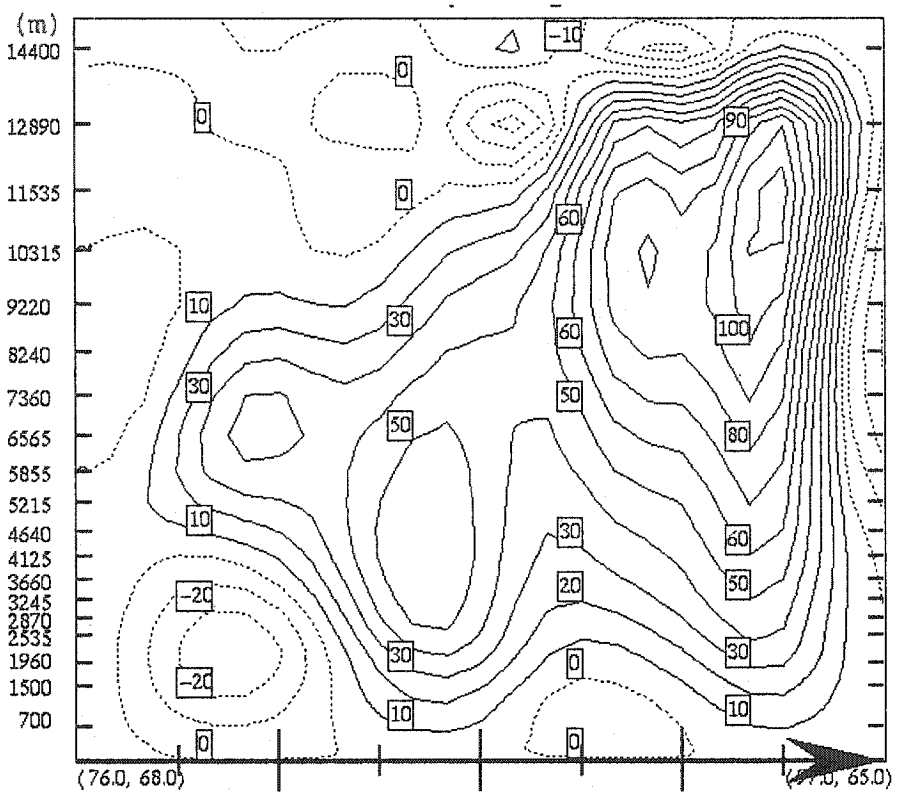

Figure 4.5: Vertical cross-section of vertical velocity at intervals of 10 cm s^{-1} through the modelled derecho at 1200 UTC 4 July. Negative values are indicated by dashed contours. Location of the cross-section is shown by the arrow in Figure 4.4.

of potentially instability favorable for convection above the warm pool. The warm pool forms as a result of warm air and moisture advection under the inversion layer. A pool of low Θ_e(cool) air is located behind a zone of strong Θ_e gradient. An examination of a vertical cross-section of temperature (not shown) indicates a cold air intrusion from the 500 hPa extending downwards, consistent with the picture that the cool pool forms as a result of convective downdrafts and the evaporation of stratiform precipitation. The presence of both a cool and a warm pool resulted in a very strong horizontal Θ_e gradient at the 850 hPa level, where the difference is as much as 40°C over 250 km. A meso-high (Fig. 4.8(a)) occurs in the region of the cool pool, discernable from the surface to 850 hPa.

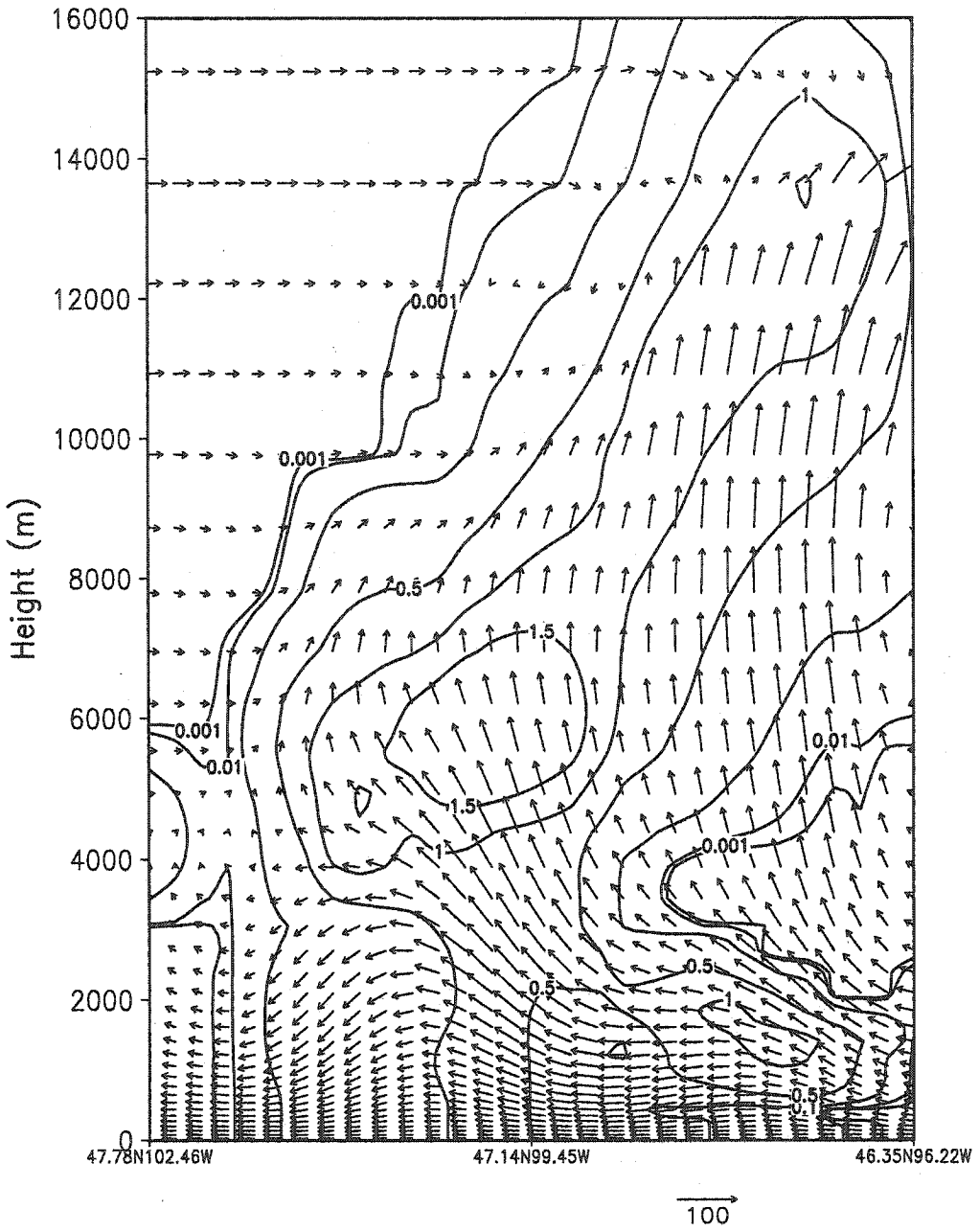

Figure 4.6: Vertical cross-section of storm relative flow (vectors in kt), and total cloud water content (solid contours) at intervals of 0.001, 0.01, 0.1, 0.5, 1.0 and 1.5 g kg^{-1} from the nested simulation at 1200 UTC 4 July. Vertical component of the wind vectors is magnified by 100 times. Location of the cross-section is shown by the arrow in Figure 4.4.

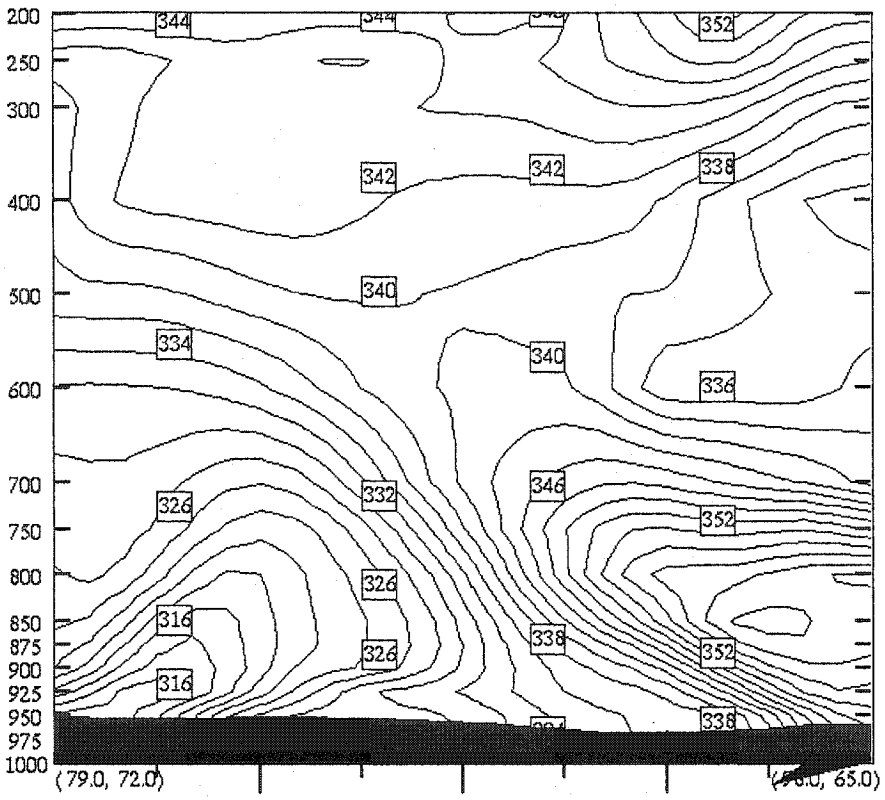

Figure 4.7: Vertical cross-section of equivalent potential temperature (Θ_e) at intervals of 2 K through the modelled derecho from the nested simulation at 1200 UTC 4 July. Location of the cross-section is shown by the thick arrow in Figure 4.10.

Figure 4.9(a) shows the simulated 500 hPa short wave trough located over Southern Manitoba and Central North Dakota at 1200 UTC July 4 1999. The position of the trough is in close agreement with the analyzed trough in Figure 4.9(b). A southward 500 hPa cold air intrusion is evident over Southeastern Manitoba, as can be inferred from the -10 and -8°C isotherms. The simulated thermal through and the associated baroclinic zone at 500 hPa are less well defined than the pattern shown in the analysis (Figure 4.9(b)). A local temperature maximum near the Central Dakotas in the simulation is associated with latent heat released by deep convection.

The 50 kt nighttime low-level jet (LLJ) at 850 hPa responsible for the Θ_e advection was captured by the model, with the nose of the LLJ just south of

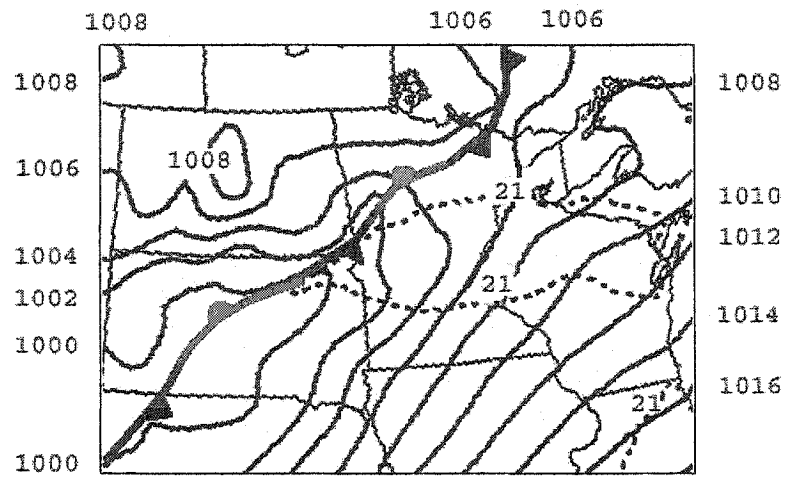

(a)

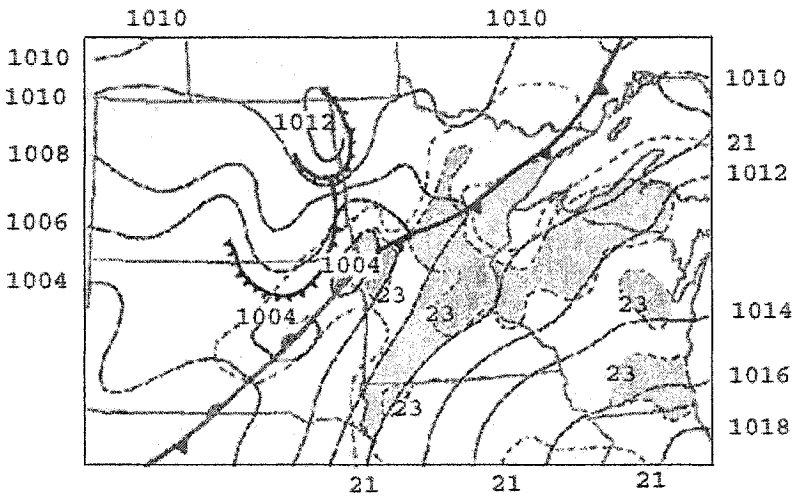

(b)

Figure 4.8: Surface analysis with positioning of surface fronts at 1200 UTC 4 July from, (a) the nested simulation, and (b) Parke and Larson (cited 2002). Isobars (solid contours) are in interval of 2 hPa, Dashed contours indicate dewpoint of 21°C, and shaded areas denote dewpoint of 23°C or greater.

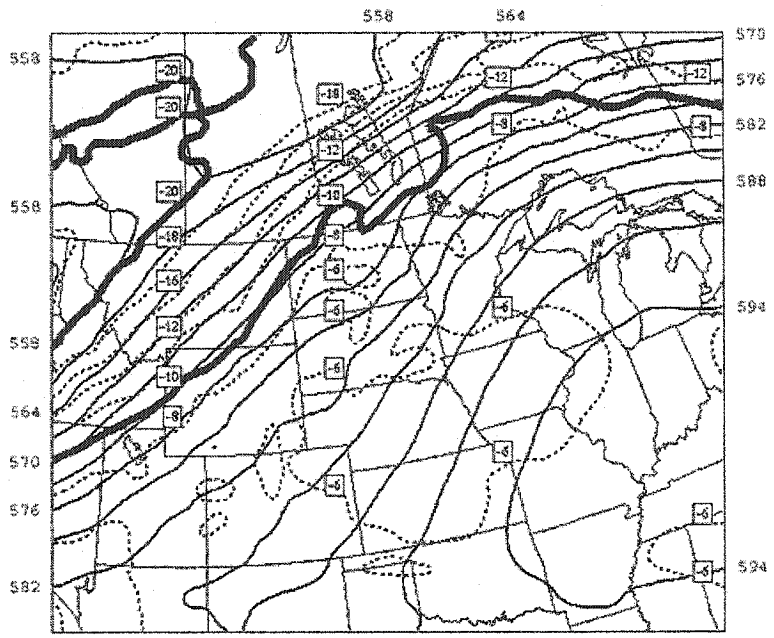

(a)

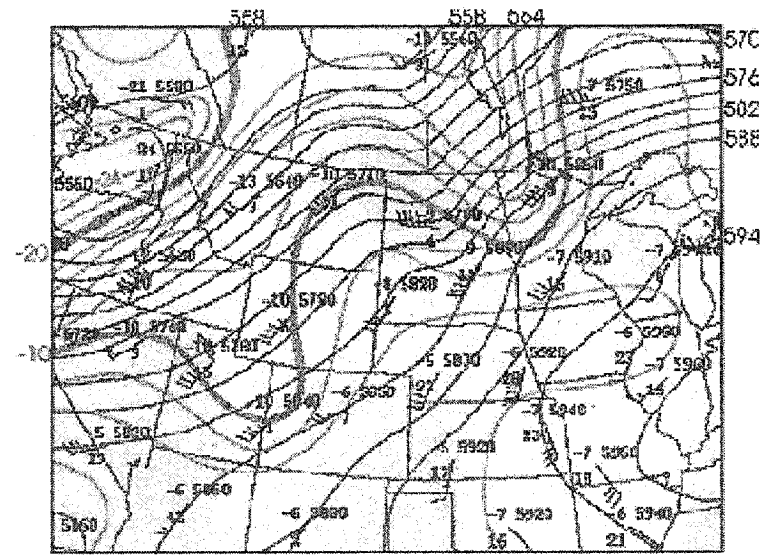

(b)

Figure 4.9: 500 hPa geopotential height at intervals of 3 dam and temperature at intervals of 2°C at 1200 UTC 4 July from, (a) the nested simulation and, (b) Parke and Larson (cited 2002).

the high Θ_e pool (Fig. 4.10). The upper-level 300 hPa jet streak that was over Idaho at 1800 UTC 3 July had advanced and stretched to formed two streaks by 1200 UTC 4 July. The leading jet maximum was over Hudson Bay and the trailing streak was located over Manitoba (Fig. 4.11). The positioning of the trailing jet streak provides the forcing for ascent over North Dakota. Another noticeable feature is that the right-entrance region of this jet streak has extended toward the location of the derecho. The simulated maximum strength of the jet was stronger than in the NCEP reanalysis by 20 to 25 kt. This difference may be partially explained by the higher resolution in the nested simulation. Nevertheless, the magnitude of the modelled jet streak is similar to the values found by Parke and Larson (cited 2002) and in the CMC regional analysis (resolution of 24 km). The location of the jet agreed well with both the NCEP and the CMC data.

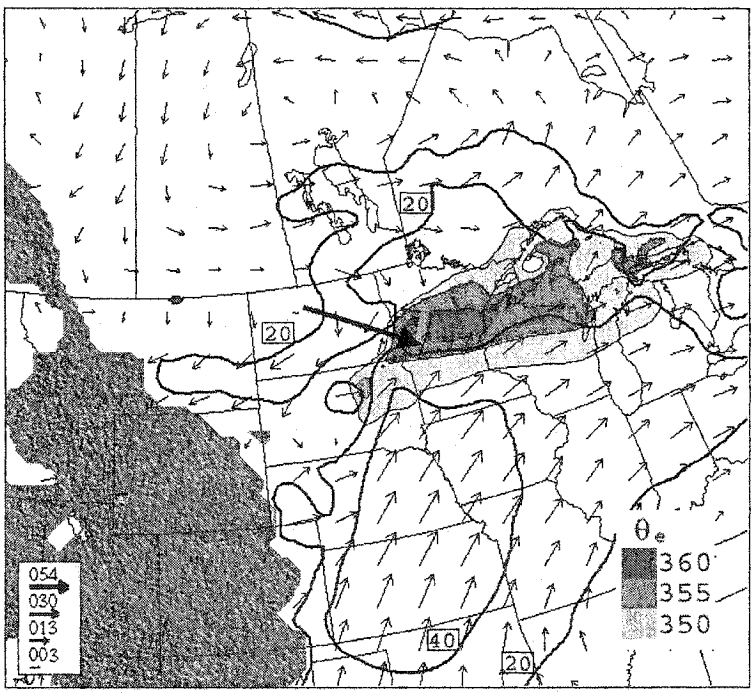

Figure 4.10: 850 hPa wind vector and wind speed (thick solid contours) at intervals of 20 kt from the nested simulation at 1200 UTC 4 July. Shaded areas indicate Θ_e of 350 K, 355 K and 360 K. Relief shading indicates area below ground. The thick arrow denotes the location of the cross-section shown in Figure 4.7.

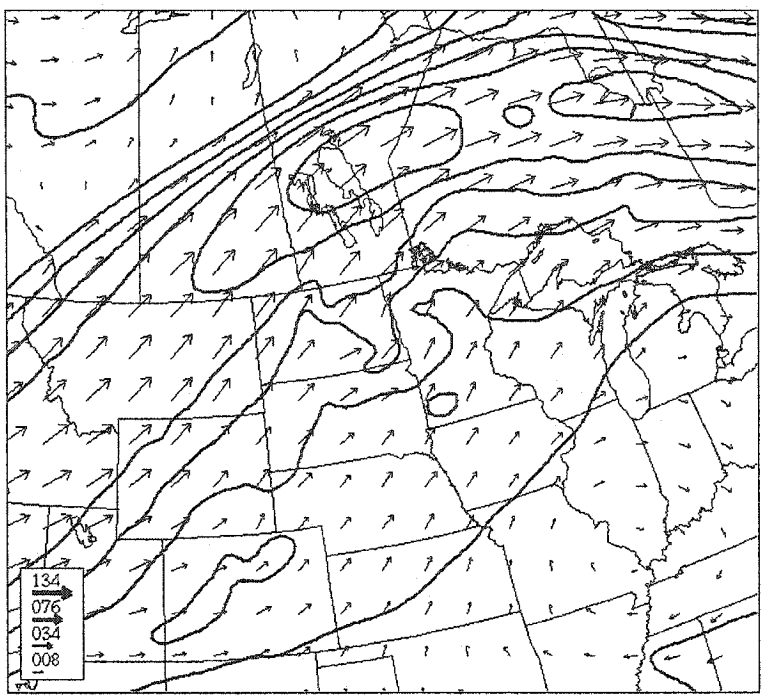

Figure 4.11: 300 hPa wind vector and wind speed contour (thick solid contours) at intervals of 20 kt from the nested simulation at 1200 UTC 4 July.

In general, the simulated surface temperatures were 2 to 4°C cooler than the observations. The force-restored surface scheme might have produced a nocturnal cooling of the surface that was too strong. A weak northeast-southwest oriented surface boundary was located at the leading edge of the strongest convective precipitation (Fig. 4.4). The temperature and the dew-point gradient across the boundary were about 4 to 5°C over 100 km, while the difference in temperature and dewpoint between the cool pool and the leading edge of the convective precipitation was about 10°C. Southeast of the boundary, the model reproduced the surface moisture pool extending from Central Minnesota into Northern Wisconsin, with dewpoints of 21 to 22°C. These values were 2 to 4°C lower than the values in the METAR reports and the analysis shown in Figure 4.8(b). As revealed in Figure 4.8(a) and 4.8(b), the important features commonly observed in squall line, such as the northeast-southwest oriented trough and the meso-high, were captured by the

model. The location of the modelled meso-high was located further west than the one observed.

To study the environment surrounding the simulated storm, comparison of modelled profiles with the nearest available upper-air soundings was made. At 1200 UTC, the derecho was located within the triangle formed by the stations Bismarck (BIS), Aberdeen (ABR), and International Falls (INL). Overall, the modelled temperature and dewpoint profiles in the mid-to-upper troposphere compared well with the radiosonde measurements (Fig. 4.12). The simulated INL sounding has the temperature structure very well captured, but the dewpoint profile is dryer than the observation above the boundary layer. At BIS and ABR, the modelled temperature was cooler and the humidity was higher in the lower troposphere. This is likely the effect of low-to-mid level clouds that were advected with the derecho over these points, along with the possible excessive nocturnal surface cooling as mentioned earlier. Both the observed soundings at ABR and INL had a deep near adiabatic layer in the troposphere from 800-600 hPa to 450-500 hPa. The simulated temperature lapse rate was less pronounced, and may be caused by the decrease in vertical resolution in Gal-Chen vertical coordinate above the boundary layer.

4.2.2 Second Stage of the Derecho and its Passage over Montreal

The observed storm began its second derecho stage near the Ontario-Quebec border at around 0100 UTC 5 July. Here we used the McGill radar data to verify the precipitation pattern of ID2. We converted the simulated rain rate into radar reflectivity using the Marshall-Palmer Z-R relation em-

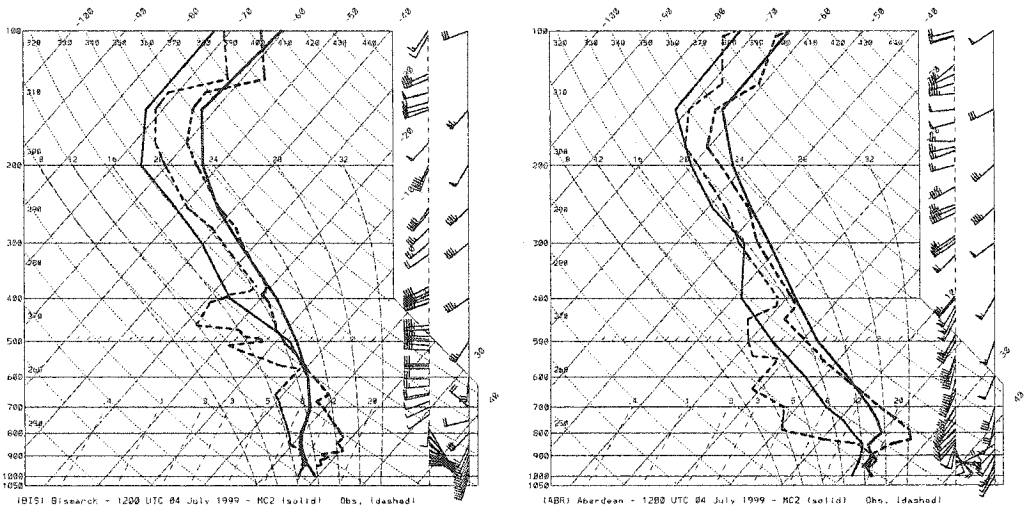

(a) (b)

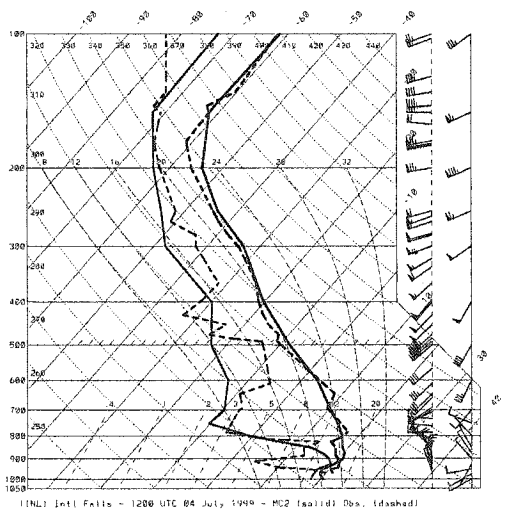

(c)

Figure 4.12: Sounding at 1200 UTC 4 July at, (a) Bismarck (BIS), (b) Aberdeen (ABR), and (c) International Falls (INL). The solid lines indicate the temperature and the dew-point profile from the nested simulation. The dashed lines indicate the observed profiles. Wind vectors are shown with the half barb, full bard, and flag denoting 5, 10, and 50 kt respectively. Location of the sounding stations are shown in Figure 2.7.

ployed by the McGill radar system (Bellon and Kilambi, 1999),

$$Z = 200R^{1.6}. \tag{4.2}$$

According to the radar map at 0600 UTC 5 July (not shown), the derecho was over the Laurentides heading toward Montreal. The simulated storm (Fig. 4.13) was moving slightly faster than the observed derecho. Therefore, a later radar imagery at 0650 UTC was chosen to compare with the modelled ID2. A bowing squall line and a trailing stratiform precipitation over the northern portion of the storm are evident from Figure 4.14(a). To obtain a scale in agreement with the resolution of the nested simulation, a 25 km $\times$ 25 km area-average of the observed radar echoes was computed (Fig. 4.14(b)). The simulated reflectivity agrees well with the coarsened values with slightly lower intensity in the modelled convective precipitation. However, since the reflectivity readings were at 2.5 km above the ground and the modelled precipitation rate used to compute the reflectivity was for the surface, it is more likely that the radar captured stronger echoes from possible hailstones at 2.5 km. The storm location was biased northward, and the orientation of the simulated squall line was rotated with respect to the radar echoes.

Figure 4.15 shows the vertical cross-section of vertical velocity. Both the strenghts of the updraft and the downdraft were weaker than the first derecho stage shown by Figure 4.5.

To investigate the storm environment prior to its arrival at Montreal, we compared the observed and the simulated soundings at Maniwaki (WMW) at 0000 UTC 5 July (Fig. 4.16). At this time, Maniwaki was the closest station to the storm and was directly in its path. The mid-to-upper level temperature profile was reasonably well simulated. The model did not capture the shallow inversion at $\sim$775 hPa. The observed dry layer at $\sim$725 hPa was found at $\sim$600 hPa in the modelled profile. The cooler boundary layer resulted in a

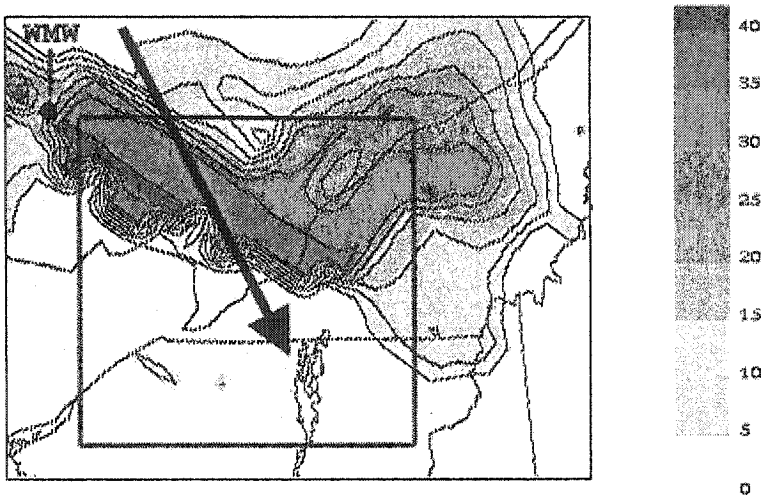

Figure 4.13: Radar reflectivity at intervals of 5 dBz computed from the modelled precipitation rate of the nested simulation for 0600 UTC 5 July. The inner box denotes the area covered by McGill radar in Figure 4.14. Black dot denotes the upper-air sounding station WMW. The arrow indicates the location of the cross-section shown in Figure 4.15.

lower CAPE of 201J kg^{-1}, comparing to 833 J kg^{-1} from the radiosonde. The CAPE is calculated for a parcel corresponding to a layer averaged temperature and dewpoints between 975 hPa and 925 hPa.

The discrepancy of the modelled winds direction above 300 hPa was probably caused by the NCEP reanalysis used to perform the coarse run. In the NCEP reanalysis data at 0600 UTC 5 July, the upper-level winds over Maniwaki are mainly westerlies (Fig. 4.16(b)). Similar winds direction was also found in the CMC analysis data. A modelled sounding taken 50 km southwest of Maniwaki (Fig. 4.16(c)) shows a temperature profile similar to the observed profile at Maniwaki, with an near isothermal layer between 750 and 700 hPa. The CAPE of 211 J kg^{-1} is of the same order as the simulated profiles at Maniwaki.

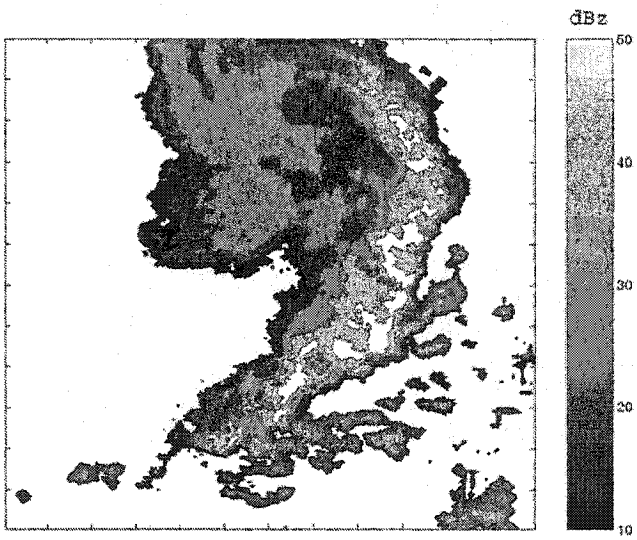

(a)

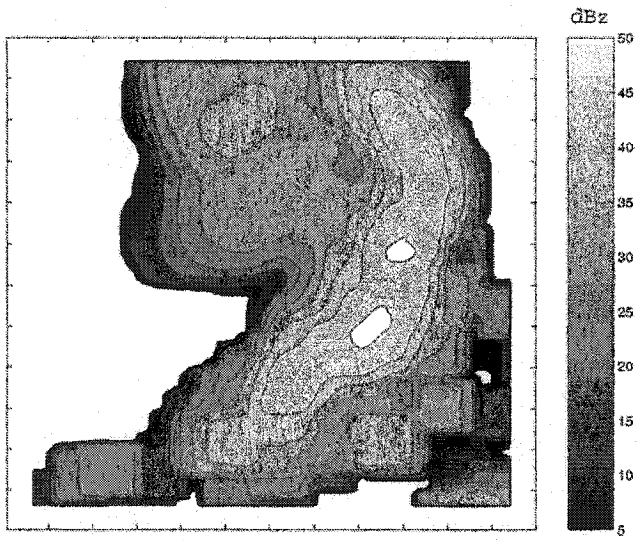

(b)

Figure 4.14: Constant-altitude plan position indicator (CAPPI) at 2.5 km elevation from McGill radar at 0650 UTC 5 July at (a) 1 km horizontal resolution at intervals of 10 dBz, and for (b) 25 km $\times$ 25 km area average at intervals of 5 dBz.

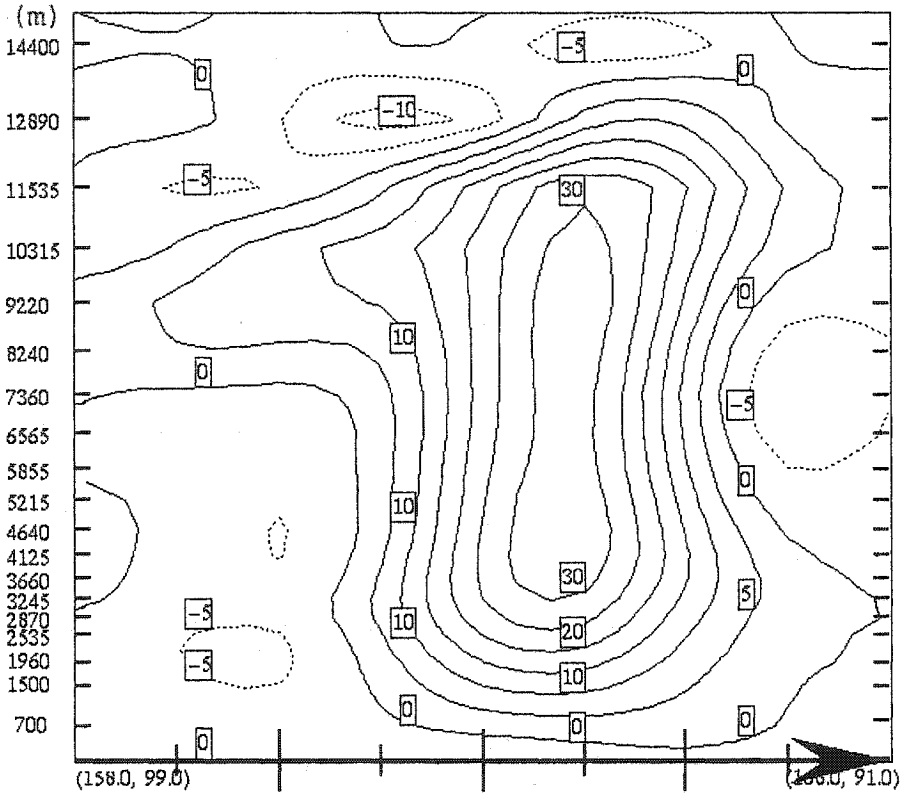

Figure 4.15: Vertical cross-section of vertical velocity at intervals of 5 cm s^{-1} through the modelled derecho from the nested simulation at 0600 UTC 5 July. The location of the cross-section is shown by the arrow in Figure 4.13.

4.2.3 Environmental Profile and Wet Microburst

It has been documented in the past that microbursts were often embedded inside larger scale meso-beta downbursts (Fujita and Wakimoto, 1981). Although no microburst were reported for ID2, it is conceivable that such phenomenon could have occurred. A closer examination of the Θ_e profiles from the soundings ahead of the derecho reveal some similarities between the simulated thermodynamic environment and the pre-storm profiles associated with wet microbursts that occur in humid regions (Atkins and Wakimoto, 1991; Johns and Doswell III, 1992). Atkins and Wakimoto (1991) defined a wet microburst as a microburst accompanied by direct or indirect observation of heavy precipitation. Figure 4.17 shows the morning (1200 UTC) and the

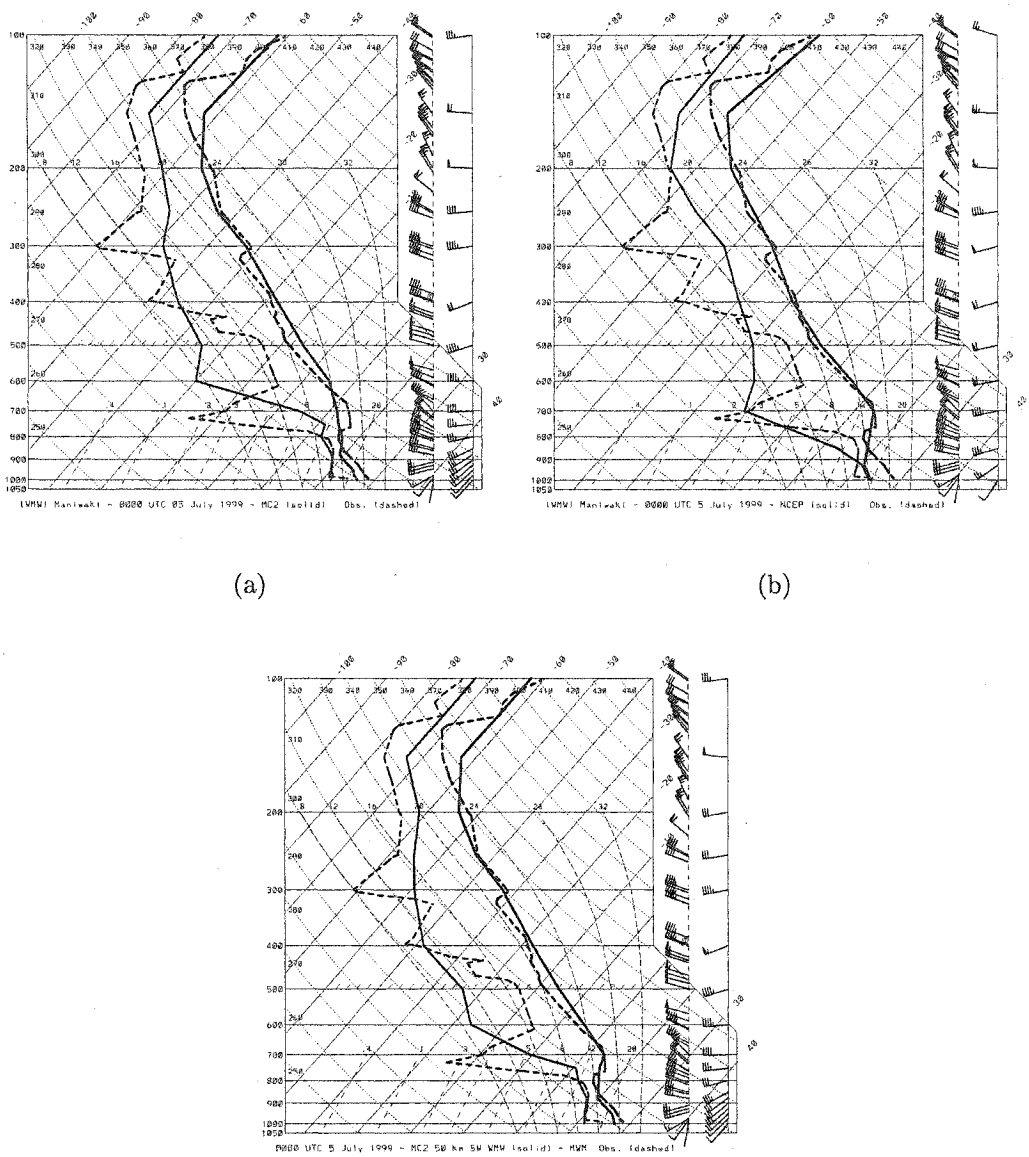

Figure 4.16: Sounding at 0000 UTC 5 July at Maniwaki (WMW). The solid lines indicate the temperature and the dewpoint profile from, (a) the nested simulation, (b) NCEP reanalysis, (C) the nested simulation at 50 km southwest of WMW. The dashed lines indicate the observed profiles at WMW. Wind vectors are shown with the half barb, full bard, and flag denoting 5, 10, and 50 kt respectively. Location of the sounding station is shown in Figure 4.13.

afternoon (1800 UTC) Θ_e environment conducive for wet microbursts from their paper. Based on observations, they computed a subjective index for potential instability using the equation,

$$\Delta\Theta_e = \Theta_{e\ min} - \Theta_{e\ max}, \tag{4.3}$$

where $\Theta_{e\ max}$ is the maximum Θ_e at or just above the surface, and $\Theta_{e\ min}$ is the minimum Θ_e found at mid-level. Their studies suggested that the difference in Θ_e between the surface and the mid-level in the afternoon is often greater than 20°C when wet microburst occurs. A $\Delta\Theta_e$ of 20°C is therefore considered the critical threshold. They also showed that the maximum Θ_e is located at the level of maximum thermal inversion in the morning, and the corresponding $\Delta\Theta_e$ is around 20°C.

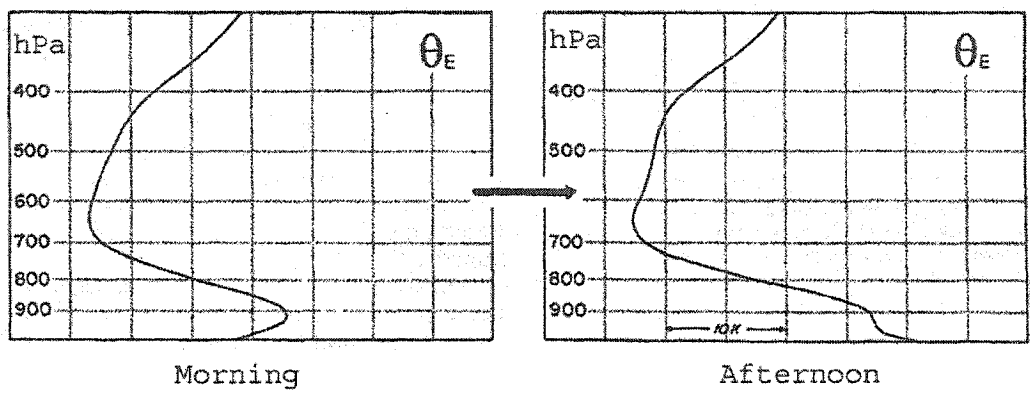

Figure 4.17: Morning (1200 UTC) and afternoon (1800 UTC) Θ_e profile for an environment conducive to wet microbursts development (Atkins and Wakimoto (1991)).

At 1200 UTC 4 July, INL, located north of the track of the derecho, was the closest sounding station to the storm. The observed and the modelled Θ_e profile are shown in Figure 4.18. The discrepancy in the low levels arises from a moister boundary layer in the simulation, as illustrated in Figure 4.12(c). In the low-to-mid levels, two shallow, potentially unstable layers were found in the observation, whereas the model generated a deeper unstable layer between 900 and 750 hPa. Note that the simulated profile exhibits features similar to

that found in a pre-microburst environment. Indeed, the $\Delta\Theta_e$ for both the modelled and observed environment at INL were above the critical threshold of 20°C, thereby potentially favorable for wet microbursts. To obtain a representative vertical structure of the environment along the storm track at the time, an average profile was computed from eight points ahead of the storm spaced every 0.5° longitude, along the latitude of 47°30'N. The vertical structure of the averaged profile displays strong potential instability for a deep column of air from 850 to 600 hPa, with a $\Delta\Theta_e$ close to 25 K. Furthermore, the column between 600 and 400 hPa was nearly potentially neutral, which would enable an initially buoyant air parcel to ascent beyond 600 hPa.

According to Atkins and Wakimoto (1991), the potential for the development of microbursts is high when the following three indices of instability are large: CAPE, lifted index, and $\Delta\Theta_e$. Table 4.1 contains a summary of the average values found in their project compared to the values from our nested simulation. Our average CAPE was lower than their morning value by about 20%, but the $\Delta\Theta_e$ and lifted index computed from our simulated environment were comparable to their afternoon values.

	Time (UTC)	$\Delta\Theta_e$ (K)	Lifted Index (K)	CAPE (J kg^{-1})
Atkins and Wakimoto (1991)	1200	18.4	-4.3	1707
	1800	26.0	-5.2	2327
ID2	1200	24.2	-6.6	1358

Table 4.1: Average values of $\Delta\Theta_e$, lifted index, and CAPE from the study by Atkins and Wakimoto (1991) and our nested simulation (ID2).

Based in part on the work from Atkins and Wakimoto (1991), the U.S. 45th Weather Squadron and the Applied Meteorology Unit (AMU) developed the Microburst-Day Potential Index (MDPI) (AMU, cited 2002; Dickerson, 2000). The index provides an outlook of wet microburst potential with a lead

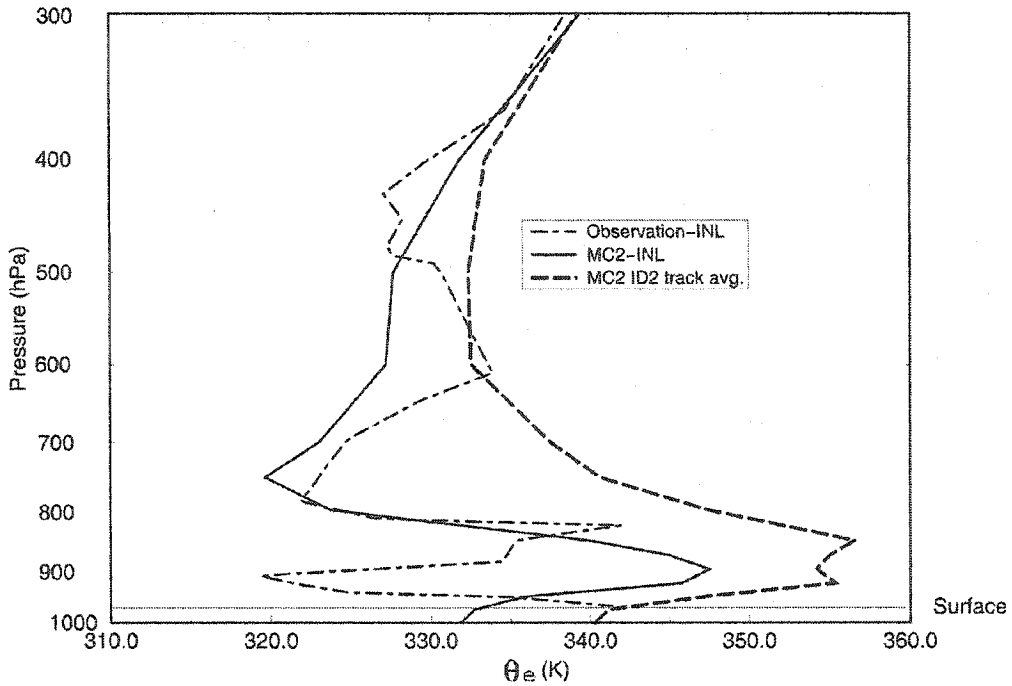

Figure 4.18: Vertical Θ_e profile (K) at 1200 UTC 4 July for International Falls (INL) from the radiosonde (dashed-dotted), the nested simulation (solid), and the modelled storm track average (dashed) using 8 vertical profiles spaced by 0.5° latitude at 47°30'N.

time of several hours. However, it is not by itself an indicator of thunderstorm potential. The equation for MDPI is,

$$MDPI = \frac{\Theta_{e\ max} - \Theta_{e\ min}}{CT}, \tag{4.4}$$

where $\Theta_{e\ max}$ is the maximum Θ_e between the surface and the lowest 150 hPa, $\Theta_{e\ min}$ is the minimum Θ_e between 650 and 500 hPa, and CT is the critical threshold which has been defined as 30 K. The likelihood of wet microbursts is high with MDPI values of one or greater, only if thunderstorm development would occur.

Figure 4.19 shows the model MDPI values at 1200 UTC and 1800 UTC 4 July, and 0000 UTC and 0300 UTC 5 July. Ahead of the derecho, MDPI values of one or greater cover a limited area over Central Minnesota and Eastern Lake Superior. Coincidentally, some of the locations where gusts over 50 kt were reported in the hours after 1200 UTC 4 July were within or

adjacent to this area of high MDPI. The potential for wet microburst was low over the Quebec, as the index remains below one for the four times. To compare with the results from Atkins and Wakimoto (1991), we relaxed CT to 20 K. We note that the area ahead of the storm is covered with relaxed MDPI value of one or greater throughout the times (Fig. 4.20). In addition, a comparison of Figures 4.21 and 4.20 indicates that the storm tends to be located on the edge of the relaxed MDPI value of unity.

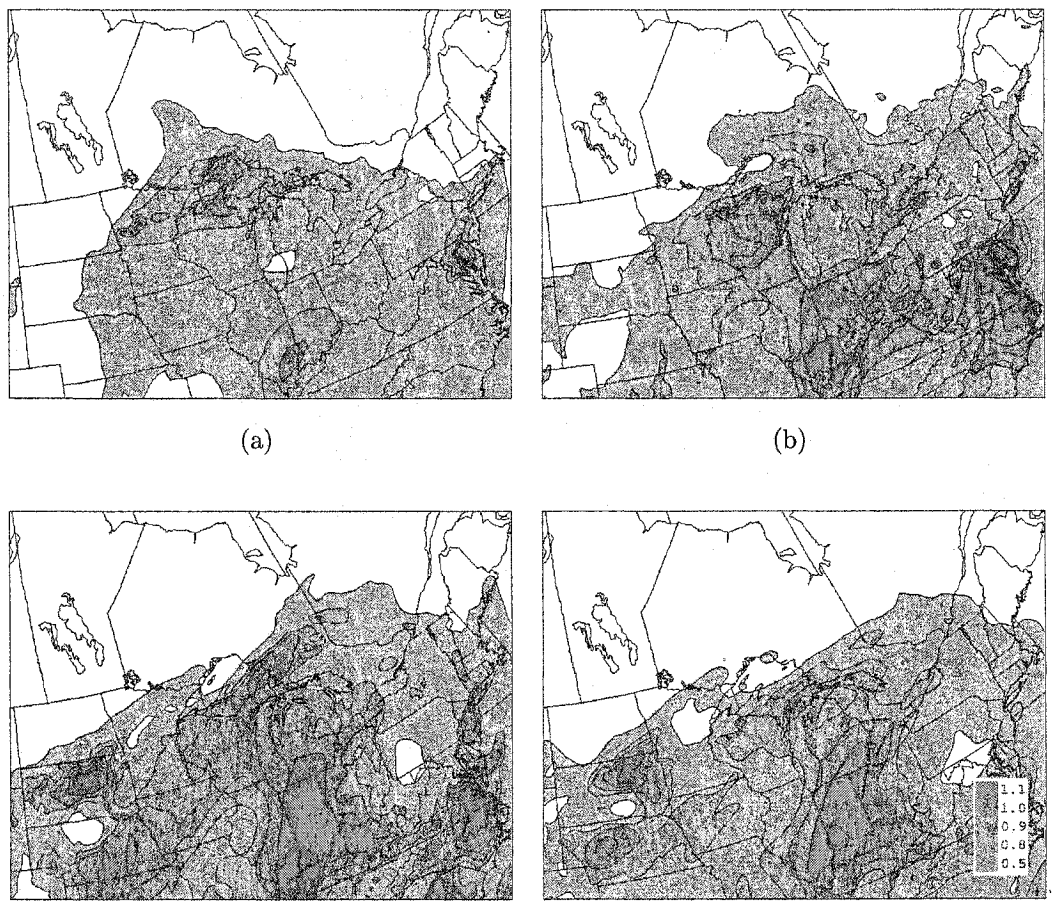

Figure 4.19: MDPI from the nested simulation at, (a) 1200 UTC 4 July, (b) 1800 UTC 4 July, (c) 0000 UTC 5 July, (d) 0300 UTC 5 July. Shadings are in interval of 0.5, 0.8, 0.9, 1.0, and 1.1.

McCann (1994) introduced a "Wind INDEX" (WINDEX) to estimate the

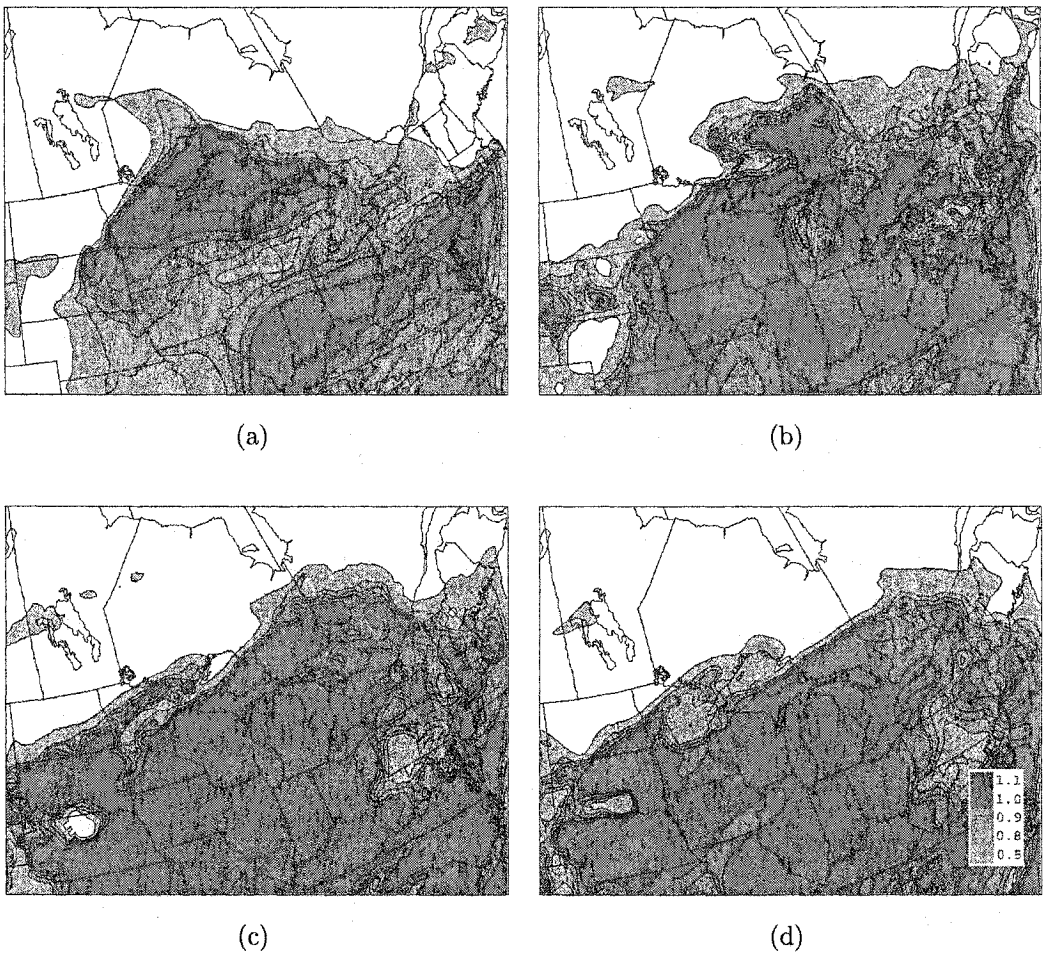

Figure 4.20: As in Figure 4.19, except the critical threshold (CT) is now set to 20 K.

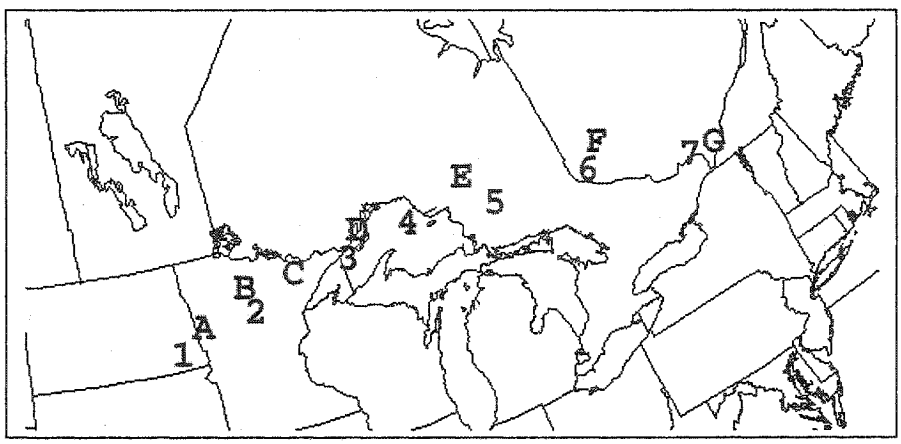

Figure 4.21: Location of the storm at every 3 hours from 1200 UTC 4 July to 0600 UTC 5 July. 1-7 denote the location from the nested simulation, and A-G denote the location from the observations.

maximum potential surface gust produced by microburst. Based on the Proctor (1989) index for microburst intensity, the WINDEX equation is given by,

$$WINDEX = 5[H_M R_Q(\Gamma^2 - 30 + Q_L - 2Q_M)]^{0.5} \tag{4.5}$$

where H_M is the height of the melting level above the ground (km), Γ is the lapse rate from the surface to the melting level (^oC km^{-1}), Q_L is the water vapor mixing ratio in the lowest one km above the surface (g kg^{-1}), Q_M is the mixing ratio at the melting level (g kg^{-1}), and $R_Q = Q_L/12$ but with a maximum value of unity. The restriction on R_Q implies that a value of the low-level mixing ratio less than 12 g kg^{-1} is insufficient to produce high precipitation storms. The radicand in Equation 4.5 may becomes negative when the lapse rate is low. In this case, WINDEX is set to zero.

The WINDEX values using the original two-level difference lapse rate (2LLR) and the thickness-weighted mean lapse rate (WMLR) are shown in Figures 4.23 and 4.24 respectively. The 2LLR is computed with the surface temperature and the height of melting level, as defined by Proctor (1989) and McCann (1994). The WMLR is calculated according to the equation,

$$\Gamma = \sum_{k=surface}^{melting\ level} -\left(\frac{z_{k+1} - z_k}{H_M}\right)\left(\frac{T(z_{k+1}) - T(z_k)}{z_{k+1} - z_k}\right), \tag{4.6}$$

where z_k is the height at level k, T is the temperature at the height z, and H_M the height of the melting level as defined previously. The term,

$$\left(\frac{z_{k+1} - z_k}{H_M}\right), \tag{4.7}$$

is the weight given for each intermediate lapse rate. Equation 4.6 can be simplified to,

$$\Gamma = \sum_{k=surface}^{melting\ level} -\left(\frac{T(z_{k+1}) - T(z_k)}{H_M}\right), \tag{4.8}$$

Because WINDEX is very sensible to the lapse rate (Γ), the difference is large between the results obtained by these two approaches.

There are no published relations between the strengths of wind gusts produced by a microburst and a derecho. Nevertheless, we would investigate if WINDEX can be useful in predicting the magnitude of wind gusts in our case. Figure 4.22 displays the location of the reported wind gusts. Table 4.2 shows the observed gusts with the corresponding maximum WINDEX values computed from the 25-km run. The values represent the maximum in a six hours period preceding each event. The results indicated that WMLR approach shows some skill estimating the gust strength over Minnesota, with difference of 10 kt or less at Moorhead, Ponsford, Hill City, and Brimson, and similarly over Quebec at Angliers, Dorval, and Frelighsburg. Generally, both methods were biased toward underestimation over Central Minnesota (location No 1-10 in Table 4.2). Overall, the estimated gusts from the 2LLR method were about half of the observations, with the exception over Eastern Ontario at Wawa, Timmins, Sudbury, and North Bay. WMLR overestimated the speeds at these same places. Given that WINDEX displays some potential in our case, it might be possible to adapt the index for derecho gusts forecasting. Since the index does not consider any local topographic effect, it may be suitable as a lower-bound for gusts potential. The overall underestimation by the 2LLR approach suggests that the estimation of the environmental lapse rate was inappropriate when the unstable layer is not surface based.

The superposition of Figure 4.21 with Figure 4.23, and Figure 4.24 reveal that the storm tends to be located near large WINDEX gradients rather than the maximum values. This is similar to the findings in microbursts, where the events tend to occur in established gradients (McCann, 1994). For microbursts, the difference between a nearby maximum and a minimum WINDEX value was generally greater than 25 kt, and the outflow from thunderstorms is the main cause for such gradient. In our derecho case, the gradient in Figure 4.24 shows similar magnitudes, and the maximum WINDEX

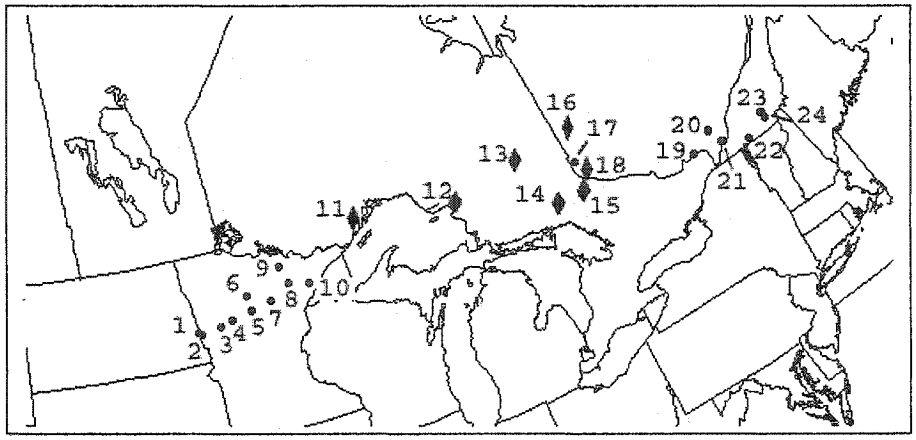

Figure 4.22: Location of wind gusts registered with the storm passage listed in Table 4.2. Dots indicate location where gusts equal to or exceed 50 kt. Rhombus indicate gusts less than 50 kt.

region tends to be located southeast of the storm. Since the index itself takes into account the instability and the low-level moisture availability, the track of a high WINDEX pool may be a useful indication of the track of the storm.

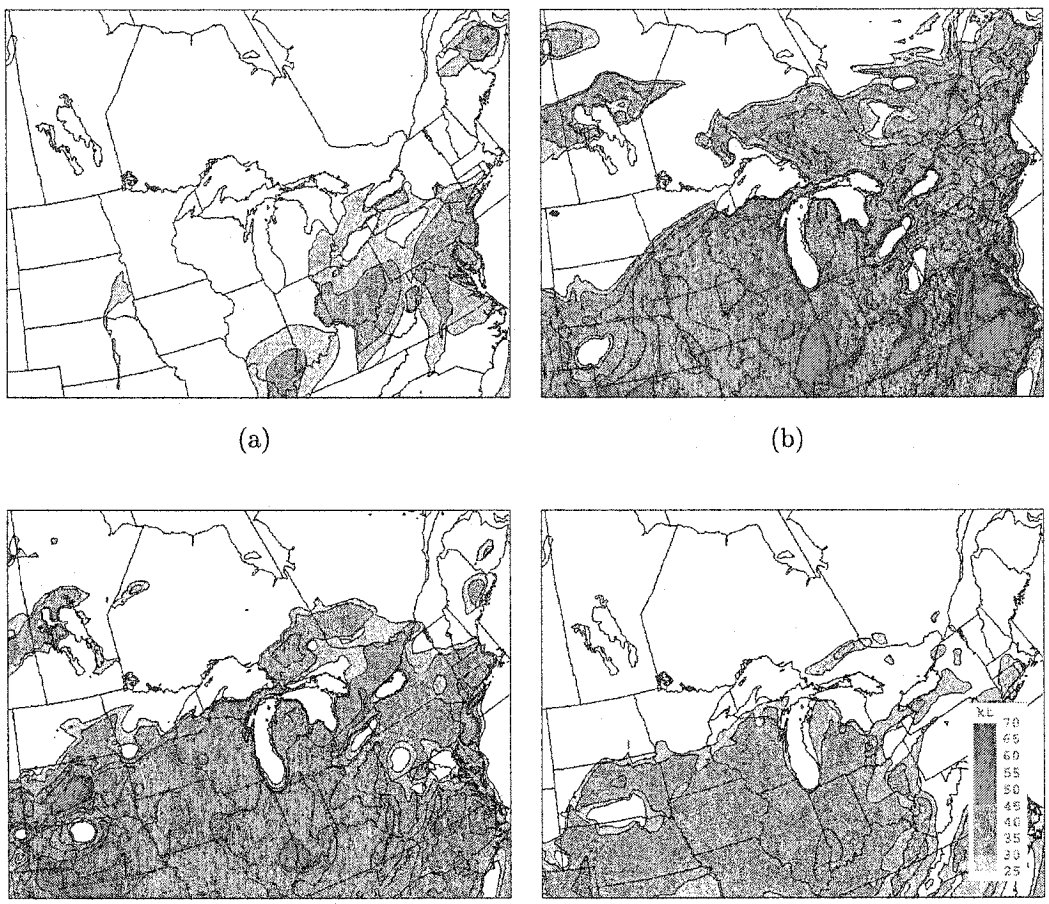

(a) (b)

(c) (d)

Figure 4.23: WINDEX from the nested simulation using the two-level difference (2LLR) method for the lapse rate at, (a) 1200 UTC 4 July, (b) 1800 UTC 4 July, (c) 0000 UTC 5 July, (d) 0300 UTC 5 July. Shadings are in interval of 5 kt starting from 25 kt.

	Observation			WINDEX	
No	Time (UTC)	Location	Gust (kt)	2LLR (kt)	WMLR (kt)
1	1242 4 July	Fargo	79	35	49
2	1245 4 July	Moorhead	56	35	49
3	1330 4 July	Detroit Lake	52	30	47
4	1413 4 July	Ponsford	52	29	47
5	1459 4 July	Walker	61	29	46
6	1500 4 July	Blackduck	65	nr	40
7	1625 4 July	Hill City	52	26	42
8	1627 4 July	Hibbing	70	27	45
	1652 4 July	Hibbing	61	nr	42
9	1630 4 July	Gheen	56	nr	42
10	1735 4 July	Brimson	52	nr	42
11	2000 4 July	Thunder Bay	40(s)	nr	nr
12	2204 4 July	Wawa	36	36	55
13	0043 5 July	Timmins	30	49	66
14	0125 5 July	Sudbury	42	38	60
15	0230 5 July	North Bay	36	38	60
16	0231 5 July	Rouyn	33	45	64
17	0230 5 July	Angliers	57	42	64
18	0235 5 July	Témiscaming	48	35	59
19	0605 5 July	Lachute	65	32	51
20	0605 5 July	St-Jérome	65	33	51
21	0630 5 July	Dorval	51	32	50
22	0708 5 July	Frelighsburg	50	nr	46
23	0744 5 July	Lennoxville	57	nr	37
24	0745 5 July	Sherbrooke	62	nr	37

Table 4.2: Summary of wind gusts registered with the storm passage from SPC and EC storm data, and surface observations. Locations are shown in Figure 4.22. (s) denotes sustained winds. WINDEX (kt) with two-level difference lapse rate (2LLR) and weighted mean lapse rate (WMLR) are shown. WINDEX less than 25 kt are reported as not relevant (nr).

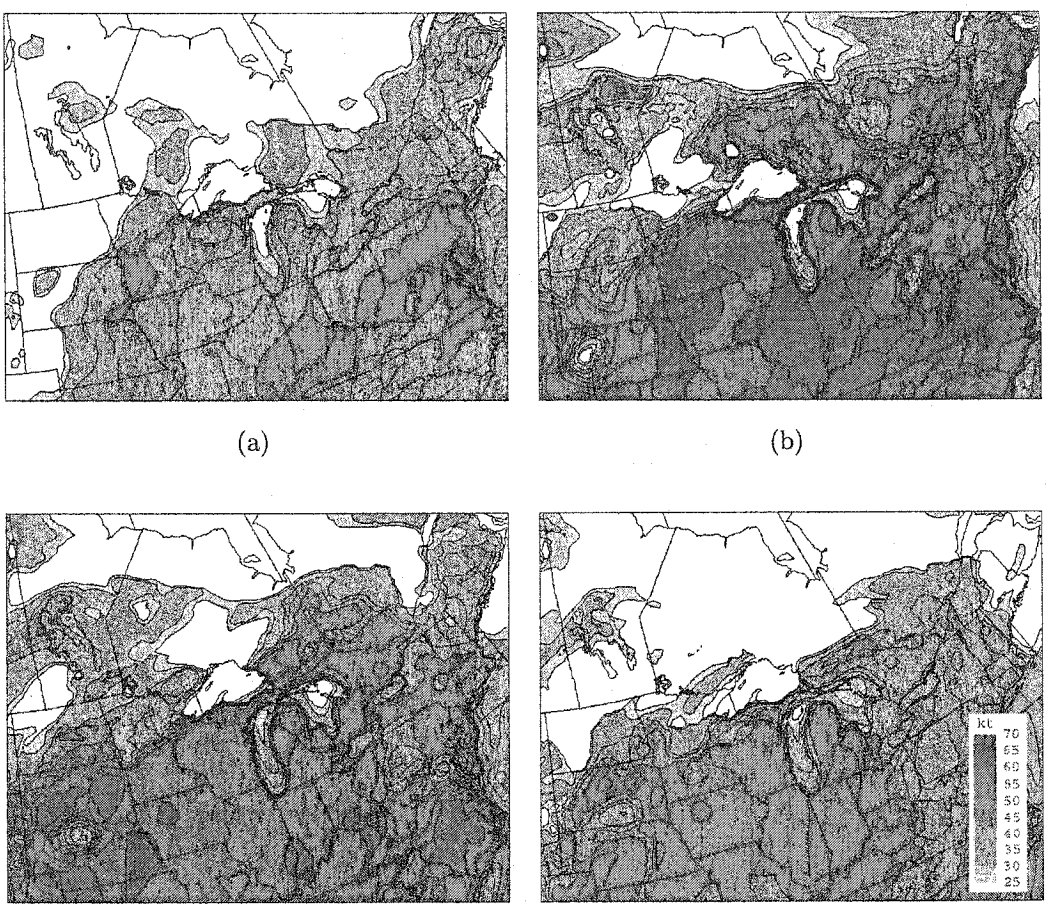

Figure 4.24: As in Figure 4.23, except the lapse rate is computed using the thickness-weighted mean (WMLR) method.

Chapter 5

Sensitivity Studies

5.1 CMC Analysis vs. NCEP Reanalysis

Numerous attempts to run the model with the CMC analyses failed to initiate deep convective cells over the observed genesis region. We have used both the regional and the global analyses extracted from the CMC archive system. The analysed fields are available on either sigma or pressure levels, and both versions have been employed with different simulation initiation times. However, none of the combinations successfully modelled the initial stage of the derecho. As shown in the last chapter, the run with the NCEP reanalysis data significantly improved the simulation results. To examine the discrepancy between the two datasets, we compared the CMC global analysis and the NCEP reanalysis, as both are available on pressure levels. Prior to the comparison, all fields were interpolated to the 80-km resolution domain.

Since the CMC runs failed to generate the storm, the environment necessary for deep convection might not be all present in this dataset. According to Johns and Doswell III (1992), the main ingredients for deep convection are the presence of, (a) moist layer in low or mid troposphere, (b) steep lapse rate

for CAPE build-up, and (c) lifting of air parcel to the level of free convection (LFC). These components will serve as the basis for determining the disparity between the NCEP and the CMC fields.

Figure 5.1 shows the difference field of 850 hPa Θ_e at 1800 UTC 3 July between the NCEP and the CMC datasets. It reveals a particularly dry layer over the South Dakota, North Dakota, and Minnesota in the CMC field. A west-east vertical cross-section of Θ_e indicates a moisture deficit extending from the surface up to 700 hPa, with the maximum difference of over 16 K near the surface (Fig. 5.2(a)). Similar features are present in a south-north cross-section over the Plains (Fig. 5.2(b)). The individual Θ_e field depicts potential instability in both datasets as Θ_e decreases with height in the low-to-mid level (not shown). However, the profile in Figure 5.2 suggests that the instability is stronger in the NCEP data due to a stronger Θ_e gradient evidenced by positive Θ_e difference in the low-level and a negative difference in the mid-level (Fig. 5.2). Hence, the atmosphere is significantly moister and more unstable for deep convection in the NCEP reanalysis.

To quantify the strength of air parcel buoyancy, the maximum lifted index (LI) was computed. The index is one of the commonly used tools for thunderstorm forecasting. It is defined as the temperature of the environment at 500 hPa minus the temperature of an air parcel when lifted moist-adiabatically to 500 hPa after it has reached the lifting condensation level (LCL) (Bluestein, 1993). Hence, as LI becomes more negative, the possibility of strong convection increases. The maximum LI is defined as the lowest LI found in a given column by lifting a parcel from a level between the surface and 700 hPa. In our case, by setting the upper level limit to 700 hPa, it ensures that all low-level moist layers were considered as a possible source of ascending air. Figure 5.3 shows the NCEP and the CMC maximum LI at 1800 UTC 3 July. The

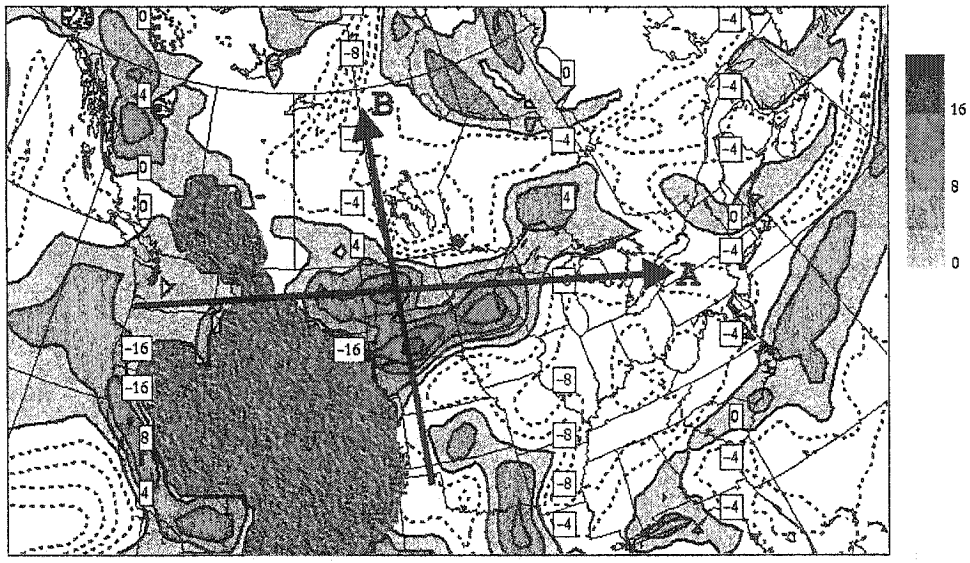

Figure 5.1: 850 hPa NCEP reanalysis Θ_e minus CMC global analysis Θ_e at intervals of 4 K at 1800 UTC 3 July. Areas of positive differences are shaded. Negative difference are in dashed contours. Relief shading indicates area below ground. The arrows A and B denote the location of the west-east and the south-north vertical cross-section shown in Figure 5.2(a) and 5.2(b) respectively.

striking feature is that a region of negative LI is located over Montana and Wyoming in the NCEP reanalysis, but the CMC analysis has positive LI over the same area. Thus there is significantly greater buoyant instability in the NCEP data over and adjacent to the area of the initiation of deep convection.

The maximum CAPE from the NCEP and the CMC data at 1800 UTC 3 July were also computed. The definition of the maximum CAPE follows that of maximum LI. It is the highest value of CAPE in an air column obtained by lifting a parcel from a level between the surface and 700 hPa. As seen in Figure 5.4, the NCEP reanalysis contains higher amount of CAPE near the foothill of the Rockies. Since convection breaks out initially over Northern Colorado and Wyoming, the smaller amount of buoyant energy over these areas in the CMC analysis significantly diminished the likelihood of initiating the observed storms.

The Q-vector divergences were computed to determine if any large scale forcing was present for lifting the air parcel. The Q-vector representation of the quasi-geostrophic ω equation is formulated as,

$$\vec{Q} = -\frac{R}{\sigma p}\left(\begin{array}{c} \frac{\partial \vec{v_g}}{\partial x}\cdot\nabla_p T \\ \frac{\partial \vec{v_g}}{\partial y}\cdot\nabla_p T \end{array}\right) \tag{5.1}$$

where $\vec{Q}$ is the Q-vector, R = 287 $Jkg^{-1}K^{-1}$ is the gas constant for dry air, $\sigma = -\frac{1}{\rho\Theta}\frac{\partial\Theta}{\partial p}$ is the static stability parameter, and $\vec{v_g}$ is the geostrophic winds (Bluestein, 1992). Since the horizontal divergence of the Q-vector is proportional to ω, sinking (rising) motion is associated with positive (negative) value of Q-vector divergence. Figure 5.5 shows the 700 to 500 hPa averaged Q-vector divergence at 1800 UTC 3 July for the two datasets. The 850 hPa level was not included in the averaging because it is mostly below ground over the Rocky Mountains. The CMC data displays large scale descending motion from Montana to Northern Colorado. On the other hand, ascending motion is present in the NCEP reanalysis over Colorado and Western Wyoming. Clearly, there is an absence of the required forcing for parcel lifting in the CMC analysis.

5.1.1 Summary

With reference to the three essential ingredients for convective development, the environment in the NCEP reanalysis is clearly more favourable for deep convection over the foothill of the Rockies foothill and over the Plains. Convection could be initiated using the NCEP data as the area of negative Q-vector divergence over the Rockies is close to the area of high CAPE over the Plains. In the CMC analysis, the lack of low-level moisture and forcing for parcel lifting significantly reduced the likelihood of convective trigger over the genesis region. The failures of our initial model runs confirmed this

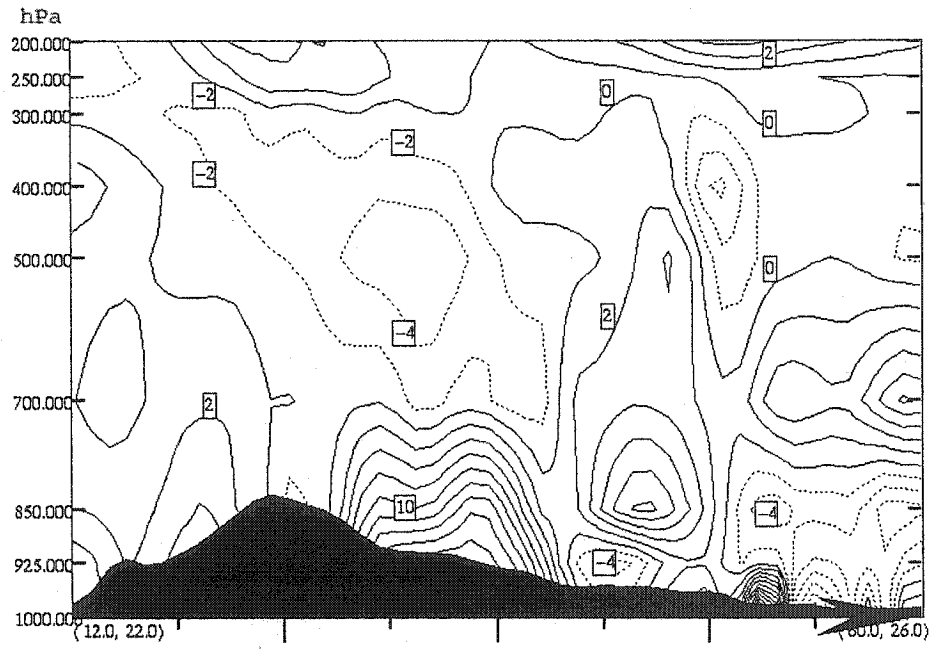

Figure 5.2: (a) West-east vertical cross-section, and (b) south-north vertical cross-section of the NCEP reanalysis Θ_e minus CMC global analysis Θ_e at intervals of 2 K at 1800 UTC 3 July. Positive differences are in solid contours and negative differences are in dashed contours. Location of the cross-section in (a) and (b) is shown by the arrow A and B respectively in Figure 5.1.

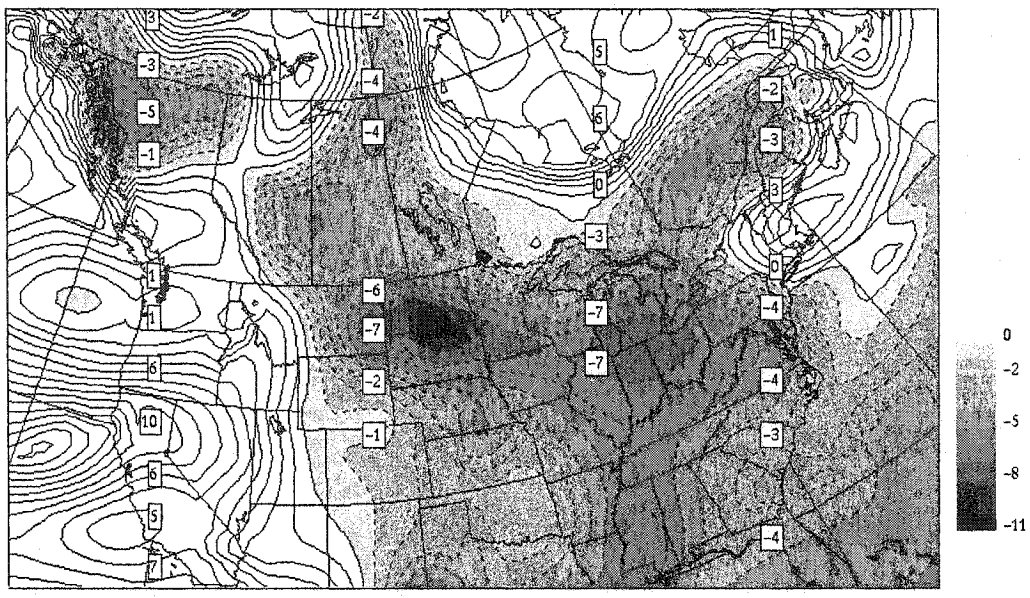

(a)

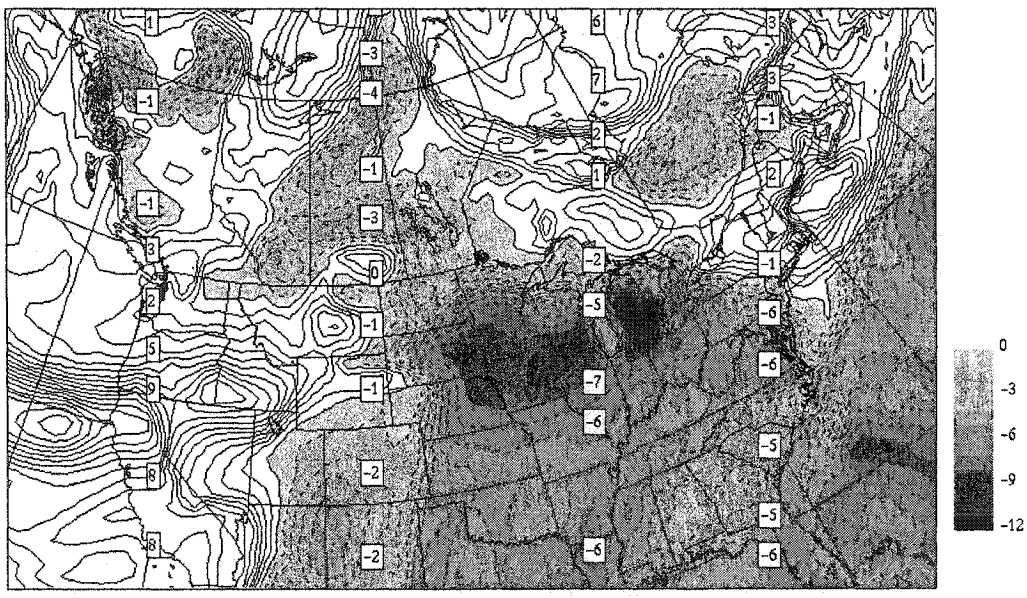

(b)

Figure 5.3: Maximum LI at 1800 UTC 3 July from, (a) NCEP reanalysis, and (b) CMC global analysis at intervals of 1 K. Positive values are in solid contours. Negative values are in dashed contours and the enclosed areas are shaded.

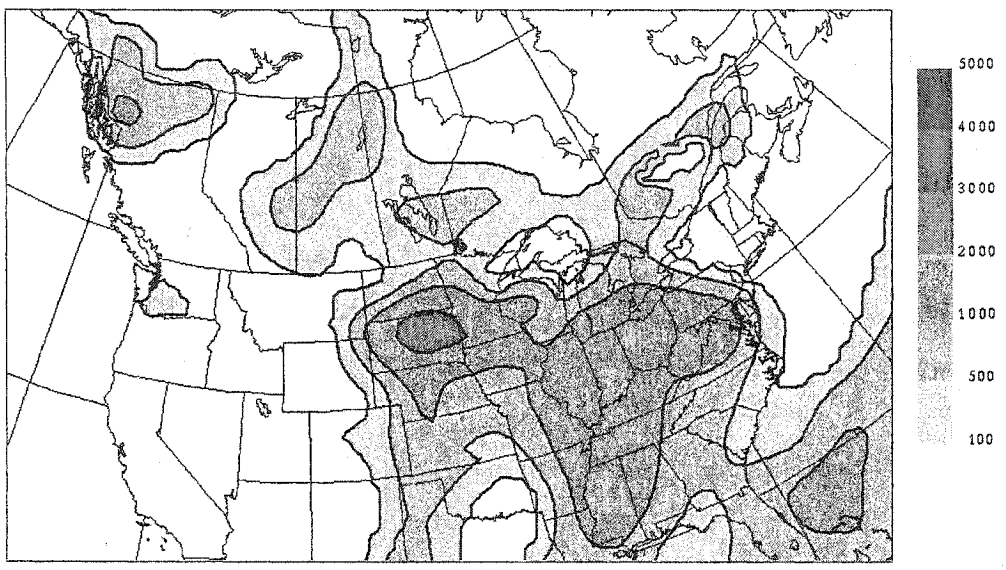

(a)

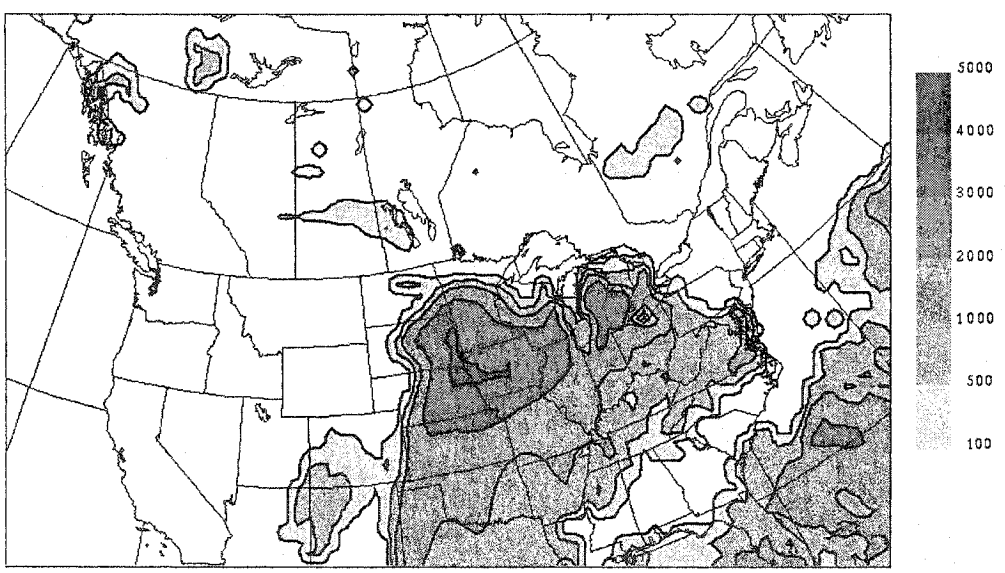

(b)

Figure 5.4: Maximum CAPE at 1800 UTC 3 July from, (a) NCEP reanalysis, and (b) CMC global analysis at intervals of 100, 500, 1000, 2000, 3000, and 4000 J kg^{-1}.

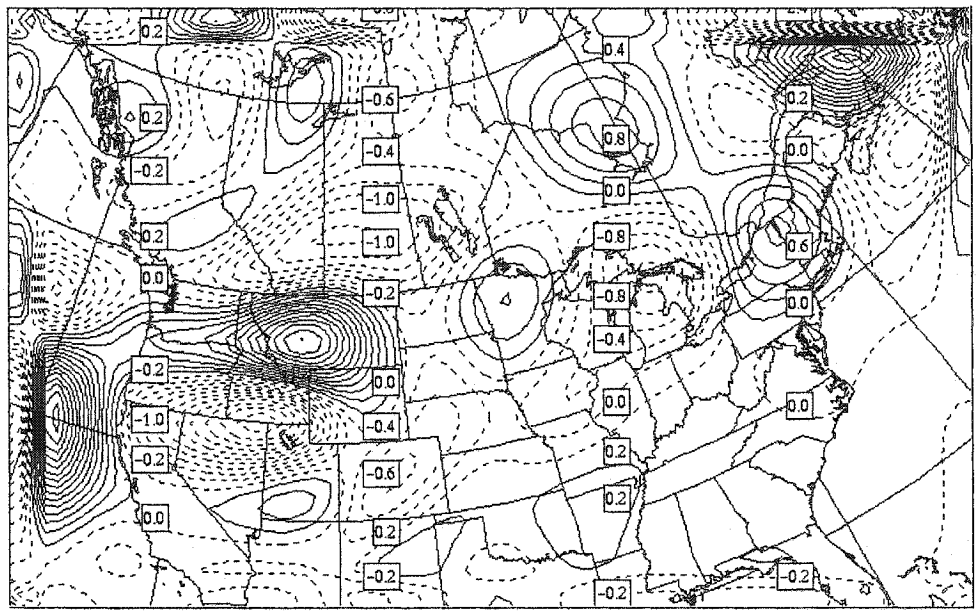

(a)

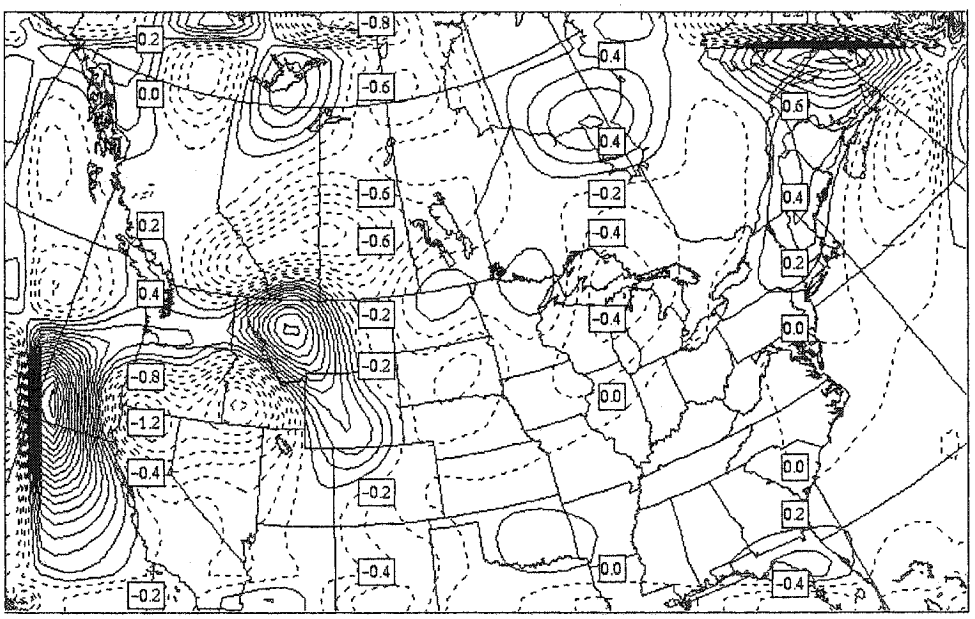

(b)

Figure 5.5: 700 to 500 hPa average Q-vector divergence at 1800 UTC 3 July from, (a) NCEP reanalysis, and (b) CMC global analysis at intervals of 0.2×10^{-12} kg m^{-2} s^{-3}. Positive values are in solid contours, and negative values are in dashed contours.

hypothesis. Hence, we used the NCEP data for our simulations.

5.2 Other Sensitivity Experiments at 25-km Resolution

Three model runs were conducted to study of the behaviour of the storm with different model settings. The sensitivity experiments employed the same domain as the one used for the 25-km simulation (REF25), and the results from REF25 served as benchmark for these sensitivity runs. The modelled profiles were also compared with radiosonde measurements. All runs started at 2100 UTC 3 July, using the outputs from the coarse run as initial and boundary conditions.

5.2.1 Effect of Shallow Convection

To assess how vertical heat and moisture transports by non-precipitating shallow clouds affect the initiation and the evolution of the simulated storm, a model run without the shallow convection scheme (SHALNIL) was performed. Except that the Betts-Miller shallow convection scheme was turned off, all other settings remain identical to REF25.

The major difference in this experiment is that the upper-level short wave trough associated with the storm deepened faster than in REF25. In fact, the geopotential height difference between SHALNIL and REF25 at 500 hPa was over 6 dam at the center of the trough at 1200 UTC 4 July. The stratiform (explicit) precipitation accumulation nearly doubled along the storm track, while the convective (implicit) precipitation amount were similar. The warming at upper-level due to latent heat release was greater, which explains the

difference in geopotential height. Due to the absence of vertical diffusion by non-precipitating clouds, there was an over-abundance of moisture in the low levels. In addition, the surface pressure gradient was much stronger and the storm location was biased westward. Because the perturbation in the thermal fields had a direct impact on the surrounding wind fields, the storm displacement was biased northward. Eventually, the storm deviated away from the moisture pool, and dissipated before reaching Lake Superior.

Figure 5.6 shows the model soundings and radiosonde observations at BIS, ABR, and INL at 1200 UTC 4 July. Recall that the triangle formed by these stations enclosed the observed derecho at that time. The profile at BIS displays important veering of the winds with height between 750 and 500 hPa, implying the occurrence of significant warm advection. Throughout the column, the wind fields display large differences from the radiosonde readings. Due to the westward bias of the storm, the vertical structure was poorly reproduced compared to Figure 4.12(a), and the near surface layer is cooler. At ABR, the low-level near-isothermal layer in Figure 5.6(b) was better reproduced than in Figure 4.12(b) from REF25. However, the shallow moist boundary layer seems to be absent, and the mid-to-upper layer is drier than the observation and REF25. Similar to Figure 4.12(c), the model resolved well the temperature profile at INL. Contrary to Figure 4.12(c), the low-level moist layer is much deeper, but the wind directions below 700 hPa also deviate significantly from the benchmark and radiosonde readings.

5.2.2 Kuo Deep Convection Scheme

An experiment using the Kuo deep convection parameterization (KUO25) was performed to determine if the scheme would handle adequately the storm at a higher horizontal resolution of 25 km.

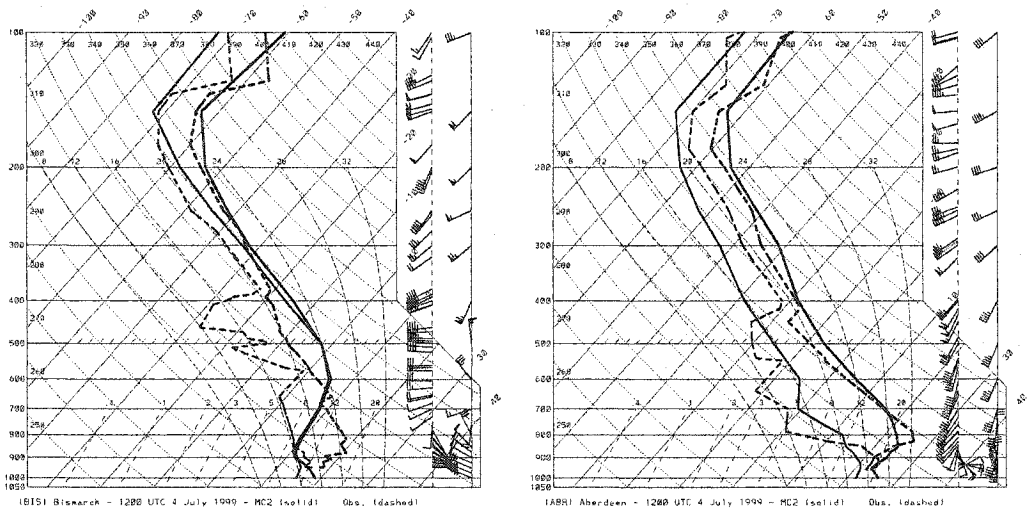

(a) (b)

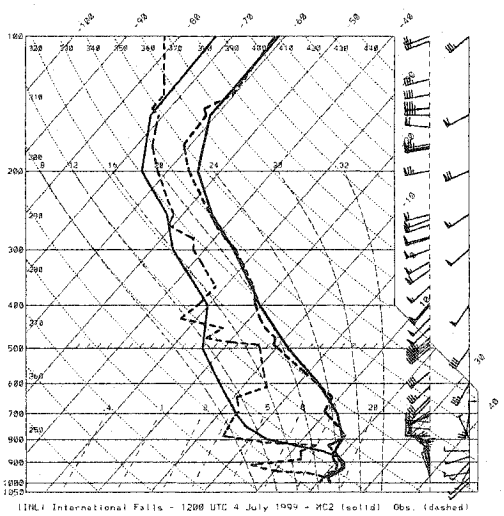

(c)

Figure 5.6: As in Figure 4.12, except for SHALNIL.

In general, the modelled storm in KUO25 propagated faster than the benchmark. By 1200 UTC 4 July, the storm had already reached Northern Minnesota. By 1800 UTC, it was located over eastern shore of Lake Superior while the actual storm has yet to reach Lake Superior at the same time (Fig. 4.21). The deep convection weakened rapidly afterwards, and dissipated before reaching the Ontario-Quebec border. The 500 hPa trough was much weaker, and the prevailing winds around the storm were more zonal than in REF25. The latter result explains the faster eastward displacement of the storm. The stratiform precipitation associated with the storm was almost nil in KUO25, which is not realistic based on station reports.

Although moving faster than other runs, the storm in KUO25 remained in the BIS-ABR-INL triangle at 1200 UTC 4 July. As Figure 5.7(a) shows, the temperature profile is well captured at BIS, and the lower troposphere is drier than all other runs. This could be explained by the fact that the column has already been convectively adjusted at the time. Otherwise, the vertical structure at ABR and INL resembled to the soundings from SHALNIL.

5.2.3 Effect of Surface Parameterization

For this experiment, the Interactions Soil-Biosphere-Atmosphere (ISBA) scheme replaced the force-restored scheme used in all other simulations. To use the ISBA scheme in MC2, several extra surface fields are required as initial conditions. Table 5.1 gives a summary of the fields required. The surface data for this simulation (ISBA25) was originally generated as part of the Mackenzie GEWEX Study (MAGS).

There were no significant differences in the evolution of the storm in ISBA25, as the storm track, the precipitation rate and accumulation were

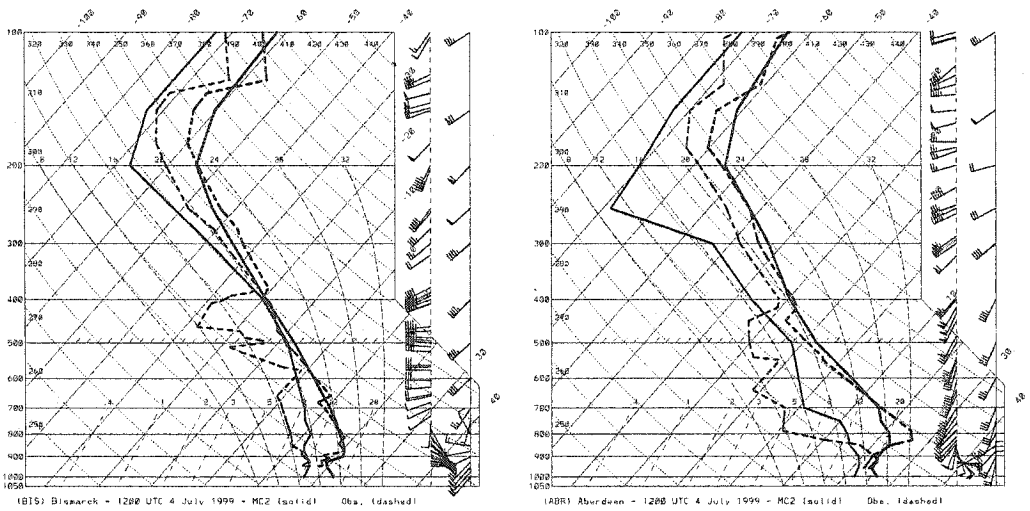

(a) (b)

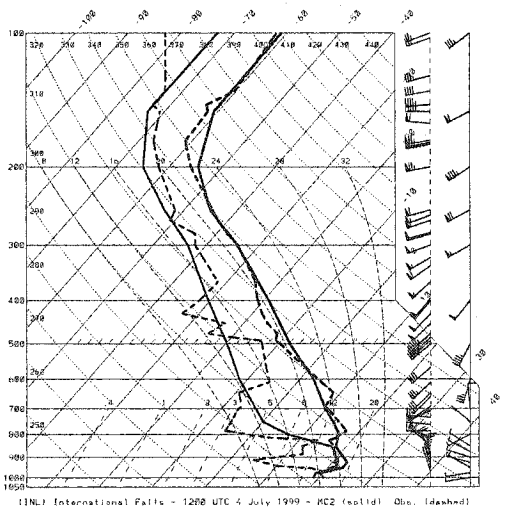

(c)

Figure 5.7: As in Figure 4.12, except for KUO25.

Field	unit
Surface temperature	K
Daily mean temperature	K
Superficial soil moisture	$m^3\ m^{-3}$
Deep soil moisture	$m^3\ m^{-3}$
Ice content in the soil	$m^3\ m^{-3}$
Vegetation fraction for 26 vegetation types	no unit
Sand fraction for the soil layer	%
Clay fraction for the soil layer	%
Snow age	h
Snow density	$kg\ m^{-3}$
Snow albedo	no unit
Liquid water retained on vegetation	$kg\ m^{-2}$
Liquid water retained in snow pack	$kg\ m^{-2}$

Table 5.1: Summary of the surface fields required for the ISBA scheme, excluding the standard geophysical fields mandatory for all surface schemes used by MC2.

similar to REF25. However, the surface temperature and specific humidity were lower than in REF25 over areas of convective downdrafts. The surface analysis at 1200 UTC 4 July discloses that ISBA25 generated an unrealistic surface cold pool with temperature below 10°C, while the stations reported temperatures between 17 and 19°C.

When compared to the soundings from all other runs, the mid-tropospheric dry layer is well reproduced at BIS, and the column is slightly drier from the surface to 600 hPa (Fig. 5.8(a)). Nevertheless, the cold bias is even more pronounced than in the benchmark and in SHALNIL near the surface. In all experiments, the winds below 800 hPa deviate from the observed direction for more than 90° at BIS. This might explain in part the disagreement in the profile at the low levels. The soundings at ABR and INL are very similar to those in REF25, but again with cooler temperature near the surface (Fig. 5.8(b), 5.8(c)). The ISBA scheme seems to cause an overcooling of the boundary layer over some areas.

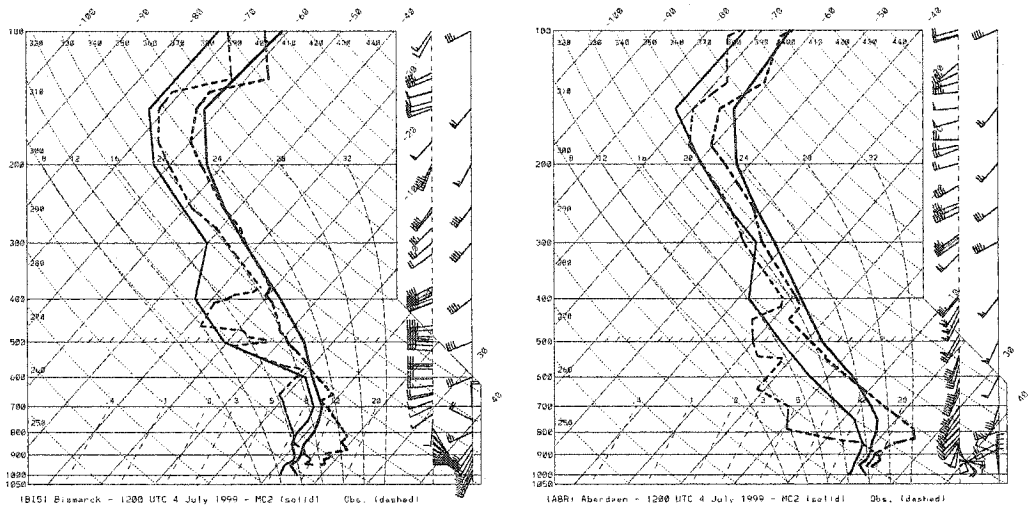

(a) (b)

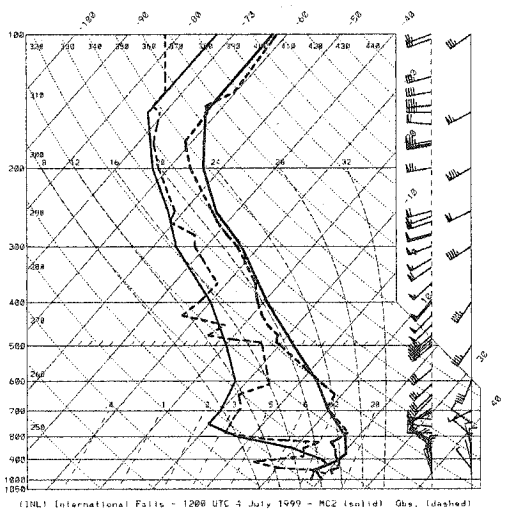

(c)

Figure 5.8: As in Figure 4.12, except for ISBA25.

5.2.4 Summary

The results confirmed that the storm is sensitive to variations in the environmental settings. The SHALNIL experiment demonstrated the importance of non-precipitating cumulus clouds which redistribute heat and moisture vertically. Without shallow convection, excessive moisture accumulation in the boundary layer resulted in incorrect simulation of the thermal winds. Although capable to trigger deep convection leading to the formation of the derecho, the large-scale Kuo deep convection scheme is not appropriated in our case at 25 km resolution as it yields an unrealistic precipitation pattern and over-estimation of storm movement. The use of the more advanced ISBA surface scheme did not significantly impacted the evolution of the modelled storm, except for a pronounced low-level cold bias over the region of convective downdrafts.

Chapter 6

Conclusion

The simulation of the long lasting and devastating 4-5 July 1999 derecho was performed using the mesoscale model MC2. The MCS left behind costly property damages, several deaths and injuries, all over a widespread area. The primary objective of this thesis is to investigate the atmospheric settings leading to the development of the derecho, and to demonstrate the capability of MC2 in simulating the observed storm. Since derechos are rare over Canada, and the operational models failed to predict this fast-moving storm, simulation of this case is both interesting and challenging.

The analysis of the pre-storm environment at 1800 UTC 3 July revealed unseasonable synoptic conditions. The low-level southerly jet over the Plains advected moisture from the Gulf of Mexico northward, forming a strong boundary layer moisture pool at the nose of the jet. In addition, above normal precipitation occurred over the Plains to moisten the surface layer. Associated with the southwesterly flow over the Rocky Mountains, the air over the Plains at 700 hPa is unusually warm as a result of daytime solar heating and adiabatic warming, causing the build-up of strong CAPE. The inversion formed above the boundary layer acted as a lid to cap the low-level

moisture pool. As the right exit region of an upper-level jet streak lies over the Plains at this time, the associated subsidence precludes the triggering of deep convection over the moist and unstable areas. The analysis showed that the eastward movement of this jet streak in the subsequent hours provided the necessary lifting over the deep unstable region.

Using the NCEP reanalysis as initial and lateral boundary conditions, the MC2 model was able to initiate the precursor deep convection leading to the formation of the derecho. The modelled convective activities were triggered further west than the radar echoes indicated, but they eventually merged and propagated to the observed storm location over North Dakota. A comparison of the modelled results and the analysis indicated that the model captured well the upper-level jet streak, short-wave trough, cold air intrusion, and the surface fields. An analysis of the distribution of Θ_e demonstrated the role played by the moisture pool and the potential instability in supporting the storm.

The second stage of the derecho over Quebec was reasonably well simulated despite the fact that the modelled storm moved slightly faster than the radar data indicated. Modelled precipitation intensity was comparable to the coarsened radar reflectivity at 25 km resolution. The vertical motion at this stage was weaker than the first derecho stage. The upper-level winds in the NCEP reanalysis were found to be responsible for the discrepancy between the modelled upper-level winds and the sounding data.

Although no microburst was reported with the storm passage, similarities were found between the simulated storm surroundings and the environment conducive to wet microburst. The original and a modified version of Microburst-Day Potential Index (MDPI) and a "Wind INDEX" (WINDEX) were computed. The results showed that the derecho tends to be located at

the edge with a relaxed MDPI value of one. We also attempted to estimate the wind gusts of the derecho using the WINDEX, and found that its value may be suitable as a lower bound estimate of the wind gust speed. The analysis of the WINDEX field further demonstrated the potential of predicting the track of the derecho by following the zone of strong WINDEX gradient and the displacement of the maximum WINDEX pool. More extensive studies would be required to confirm these results.

A number of sensitivity experiments were also carried out. Initially, the CMC analyses were used as initial and lateral boundary conditions for the simulations. However, we were not able to simulate the initial stage of the derecho in this manner. A comparison between the CMC and the NCEP analyses at 1800 UTC 3 July revealed that over and adjacent to the area where deep convection was initiated, the environment depicted in the NCEP reanalysis exhibits a significantly moister troposphere, as well as higher potential instability for deep convection. Furthermore, the CMC analysis displayed large-scale descent from Montana to Northern Colorado while ascending motion was present in the NCEP reanalysis over Colorado and Western Wyoming. Other sensitivity experiments demonstrated that, a) without shallow convection, there is an excessive accumulation of moisture in the boundary layer, b) the Kuo deep convective scheme resulted in a unrealistic precipitation pattern and an over-estimation of the motion of the storm, and c) the use of the ISBA surface scheme did not significantly affect the evolution of the storm but generated a too strong cold pool in regions associated with convective downdrafts.

Bibliography

AMU, cited 2002: Applied Meteorology Unit Quarterly Update Report, Fourth Quarter FY-95. [Available online at http://technology.ksc.nasa.gov/WWWaccess/AMU/4th95/4th_quarter95.html].

Atkins, N. T. and R. M. Wakimoto, 1991: Wet microburst acitvity over the Southeastern United States: Implications for forecasting. *Wea. Forecasting*, **6**, 470–482.

Bellon, A. and A. Kilambi, 1999: Updates to the McGill RAPID (Radar Data Analysis, Processing and Interactive Display) system. *29th Conf. on Radar Meteor.*, Montreal, Canada, Amer. Meteor. Soc., 121-124 .

Benoit, R., J. Côté, and J. Mailhot, 1989: Inclusion of a TKE boundary layer parameterization in the Canadian regional finite-element model. *Mon. Wea. Rev.*, **117**, 1726–1750.

Benoit, R., M. Desgagné, P. Pellerin, S. Pellerin, Y. Chartier, and S. Desjardins, 1997: The Canadian MC2: A semi-Lagrangian, semi-implicit wideband atmospheric model suited for finescale process studies and simulation. *Mon. Wea. Rev.*, **125**, 2382–2415.

Bentley, M. L. and S. R. Cooper, 1997: The 8 and 9 July 1993 Nebraska derecho: An observational study and comparison to the climatology of related mesoscale convective systems. *Wea. Forecasting*, **12**, 678–688.

Bentley, M. L. and T. L. Mote, 1998: A climatology of derecho-producing mesoscale convective systems in the Central and Eastern United State, 1986-1995. Part I: Temporal and spatial distribution. *Bull. Amer. Met. Soc.*, **79**, 2527–2540.

Bernardet, L. R. and W. R. Cotton, 1998: Multiscale evolution of a derecho-producing mesoscale convective system. *Mon. Wea. Rev.*, **126**, 2991–3015.

Betts, A. K. and M. J. Miller, 1993: The Betts-Miller scheme. *The Representation of Cumulus Convection in Numerical Models, Meteor. Monogr.*, **24**, 107–121.

Bluestein, Howard B., 1992: *Synoptic-Dynamic Meteorology in Midlatitudes*, volume I. Oxford University Press, 431 pp.

Bluestein, Howard B., 1993: *Synoptic-Dynamic Meteorology in Midlatitudes*, volume II. Oxford University Press, 594 pp.

Coniglio, M. C. and D. J. Stensrud, 2001: Simulation of progressive derecho using composite initial conditions. *Mon. Wea. Rev.*, **129**, 1593–1616.

Dickerson, S. N., 2000: An evaluation of microburst prediction indices for the Kennedy Space Center and Cape Canaveral Air Station (KSC/CCAS). Master's thesis, Air University, Wright-Patterson Air Force Base, OH 45433, United States. [Available online at https://research.maxwell.af.mil/papers/student/ay2000/afit/afit-gm-enp-00m-06.pdf].

EC, cited 2000: Top ten weather stories of 1999. [Available online at http://www.ec.gc.ca/press/10stor99_b_e.htm].

Fritsch, J. M. and J. S. Kain, 1993: Convective parameterization for mesoscale models: The Fritsch-Chappell scheme. *The Representation of Cumulus Convection in Numerical Models, Meteor. Monogr.*, **24**, 159–164.

Fujita, T. T. and R. M. Wakimoto, 1981: Five scales of airflow associated with a series of downbursts on 16 July 1980. *Mon. Wea. Rev.*, **109**, 1438–1456.

Fulton, R. A., J. P. Breidenbach, D. J Seo, and D. A. Miller, 1998: The WSR-88D rainfall algorithm. *Wea. Forecasting*, **13**, 377–395.

GLSEA, cited 2002: Daily lake average surface water temperature. [Available online at http://coastwatch.glerl.noaa.gov/glsea/glsea.html].

Guichard, F., D. Parsons, and E. Miller, 2000: Thermodynamic and radiative impact of the correction of sounding humidity bias in the tropics. *Journal of Climate*, **13**, 3611–3624.

Hinrichs, G., 1888: Tornadoes and derechos. *Amer. Meteor. J.*, **5**, 306–317, 341–349.

Johns, R. H. and C. A. Doswell III, 1992: Severe local storms forecasting. *Wea. Forecasting*, **7**, 588–612.

Johns, R. H. and W. D. Hirt, 1987: Derecho: Widespread convectively induced windstorms. *Wea. Forecasting*, **2**, 32–49.

Kain, J. S. and J. M. Fritsch, 1993: Convective parameterization for mesoscale models: The Kain-Fritsch scheme. *The Representation of Cumulus Convection in Numerical Models, Meteor. Monogr.*, **24**, 165–170.

Kalnay, E., M. Kanamitsu, R. Kistler, W. Collins, D. Deaven, L. Gandin, M. Iredell, S. Saha, G. White, G. Woollen, Y. Zhu, M. Chellliah, W. Ebisuzaki, W. Higgins, J. Janowiak, K. C. Mo, C. Ropelewski, J. Wang, A. Leetmaa, R. Reynolds, R. Jenne, and D. Joseph, 1996: The NCEP/NCAR 40-year reanalysis project. *Bull. Amer. Met. Soc.*, **77**, 437–471.

Kong, F. and M. K. Yau, 1997: An explicit approach to microphysics in MC2. *Atmosphere-Ocean*, **126,** 257–291.

Mailhot, J., S. Blair, R. Benoit, B. Bilodeau, Y. Delage, L. Fillion, L. Garant, C. Girard, and A. Tremblay, 1998: Scientific description of RPN physic library. Version 3.6. Technical report, Recherche en Prévision Numérique, Atmospheric Environment Service, 2121 Transcanadian, Montreal, QC H9P 1J3, Canada.

Mainville, S., R. Héroux, and P. Vaillancourt, 2001: The derecho of July 5, 1999 in Quebec: A rare event. *25th CMOS Congress*, Winnipeg, Canada, Canadian Meteor. and Oceanogr. Soc.

McCann, D. W., 1994: WINDEX-A new index for forecasting microburst potential. *Wea. Forecasting*, **9,** 532–541.

McNulty, R. P., 1995: Severe and convective weather: A Central region forecasting challenge. *Wea. Forecasting*, **10,** 187–202.

Mitchell, H. L., Charette C., S. J. Lambert, J. Hallé, and C. Chouinard, 1993: The Canadian global data assimilation system: Description and evaluation. *Mon. Wea. Rev.*, **121,** 1467–1492.

Mitchell, H. L., C. Chouinard, C. Charette, , R. Hogue, and S. J. Lambert, 1996: Impact of a revised analysis algorithm on a operational data assimilation system. *Mon. Wea. Rev.*, **124,** 1243–1255.

NCDC, cited 2002a: July 1999 climate report for the Midwest region. [Available online at http://lwf.ncdc.noaa.gov/oa/pub/data/special/july-99-mrcc.html].

NCDC, cited 2002b: U.S. Climate at a glance. [Available online at http://lwf.ncdc.noaa.gov/oa/climate/research/cag3/cag3.html].

Noilhan, J. and S. Planton, 1989: A simple parameterization of land surface processes for meteorological models. *Mon. Wea. Rev.*, **117**, 536–549.

Parke, P. S. and N. J. Larson, cited 2002: The Boundary Waters windstrom of July 4, 1999. [Available online at http://www.crh.noaa.gov/dlh/science/index.html].

Proctor, F. H., 1989: Numerical simulations of an isolated microburt. Part II: Sensitivity experiments. *Journal of Atmospheric Sciences*, **46**, 2143–2165.

SPC, cited 2002: Forecast Archive. [Available online at http://www.spc.noaa.gov/archive/products/].

WESO, 2002. Storm damages reports and weather bulletins. Meteorological and environmental service office at Montreal, Meteorological service of Canada.